PAIN® 154 (2013) 1551–1568

PAIN®

www.elsevier.com/locate/pain

Upregulation of P2X3 receptors by neuronal calcium sensor protein VILIP-1 in dorsal root ganglions contributes to the bone cancer pain in rats

Min Liu [a,b], Huan Yang [a], Dong Fang [a], Jing-Jing Yang [a], Jie Cai [a,b], You Wan [a,b,c], De-Hua Chui [a,b], Ji-Sheng Han [a,b,c], Guo-Gang Xing [a,b,c,*]

[a] Neuroscience Research Institute, Peking University, Beijing, PR China
[b] Department of Neurobiology, School of Basic Medical Sciences, Peking University Health Science Center, Beijing, PR China
[c] Key Laboratory for Neuroscience, Ministry of Education and Ministry of Health, Beijing, PR China

Sponsorships or competing interests that may be relevant to content are disclosed at the end of this article.

ARTICLE INFO

Article history:
Received 16 January 2013
Received in revised form 24 March 2013
Accepted 11 April 2013

Keywords:
Bone cancer pain
Dorsal root ganglion
Hyperexcitability
Neuronal calcium sensor protein VILIP-1
P2X3 receptors

ABSTRACT

Primary and metastatic cancers that affect bone are frequently associated with severe and intractable pain. The mechanisms underlying the development of bone cancer pain are largely unknown. In this study, we first demonstrated that a functional upregulation of P2X3 receptors in dorsal root ganglion (DRG) neurons is closely associated with the neuronal hyperexcitability and the cancer-induced bone pain in MRMT-1 tumor cell–inoculated rats. Second, we revealed that visinin-like protein 1 (VILIP-1), a member of visinin-like proteins that belong to the family of neuronal calcium sensor proteins is responsible for the observed upregulation of P2X3 receptors in DRG neurons. The interaction between the amino terminus of VLIP-1 and the carboxyl terminus of the P2X3 receptor is critical for the surface expression and functional enhancement of the receptor. Finally, overexpression of VILIP-1 increases the expression of functional P2X3 receptors and enhances the neuronal excitability in naive rat DRG neurons. In contrast, knockdown of VILIP-1 inhibits the development of bone cancer pain via downregulation of P2X3 receptors and repression of DRG excitability in MRMT-1 rats. Taken together, these results suggest that functional upregulation of P2X3 receptors by VILIP-1 in DRG neurons contributes to the development of cancer-induced bone pain in MRMT-1 rats. Hence, P2X3 receptors and VILIP-1 could serve as potential targets for therapeutic interventions in cancer patients for pain management. Pharmacological blockade of P2X3 receptors or knockdown of VILIP-1 in DRGs would be used as innovative strategies for the treatment of bone cancer pain.

© 2013 International Association for the Study of Pain. Published by Elsevier B.V. All rights reserved.

1. Introduction

Bone cancer pain resulting from primary tumors or tumors that metastasize to bone is one of the most severe and intractable types of cancer pain, which decreases the quality of life of patients [20]. The mechanisms underlying the development of cancer-induced bone pain remain largely unknown.

Recently, we and others have found that the thermal hyperalgesia and mechanical hypersensitivity in murine models of bone cancer pain are associated with enhanced excitability of primary sensory dorsal root ganglion (DRG) neurons [45,46]. On the other hand, adenosine triphosphate (ATP) and its P2X purinergic receptors have been shown to depolarize DRG neurons [2] and excite the peripheral terminals of these neurons [14,34]. P2X receptors belong to a family of ligand-gated ion channels that are activated by extracellular ATP [35]. Of 7 P2X receptors (P2X1–7) identified to date [11], the P2X3 receptors are selectively expressed at high levels on small- and medium-diameter nociceptive DRG neurons, suggesting a significant role of this receptor subtype in processing pain [10,22]. Coincidently, systemic blockade of P2X3 and P2X2/3 receptors attenuates cancer-induced pain behaviors in rats [21]. Therefore, it would be reasonable to speculate that signaling events with purinergic P2X3 receptors likely contribute to the hyperexcitability of nociceptive DRG neurons, which is suggested to underlie the pathogenesis of peripheral sensitization and persistent pain under cancer condition [46]. In fact, a recent study reported a functional upregulation of P2X3 receptors in DRG

* Corresponding author. Address: Neuroscience Research Institute, Peking University, 38 Xue-Yuan Road, Beijing 100191, PR China. Tel.: +86 10 8280 1067; fax: +86 10 8280 1067.
E-mail address: ggxing@bjmu.edu.cn (G.-G. Xing).

0304-3959/$36.00 © 2013 International Association for the Study of Pain. Published by Elsevier B.V. All rights reserved.
http://dx.doi.org/10.1016/j.pain.2013.04.022

neurons in a rat model of bone cancer pain [40]. However, the underlying mechanism of such upregulation is unclear.

Visinin-like protein 1 (VILIP-1), a member of the neuronal calcium sensor protein family, has been shown to act as a modulator of the α4β2 nicotinic acetylcholine receptors (nAChRs) by increasing their surface expression and function in oocytes [27] as well as in hippocampal neurons [44]. Moreover, VILIP-1 has also been identified in a functional protein complex with glutamate receptors of the kainite subtype GluR6 [12] and in a signaling complex with P2X2 receptors in which VLIP-1 can regulate the surface expression of P2X2 and also the sensitivity and peak response to ATP [8]. VILIP-1 has been proposed to potentially function as a general regulator of ligand-gated ion channels, modulating the surface expression and function of the receptors [3,8]. We hypothesized that VILIP-1 may interact with P2X3 receptors and regulate their functional expression under cancer conditions and may ultimately contribute to the development of bone cancer pain in a rat model.

In this study, we disclosed a novel molecular mechanism underlying the functional upregulation of P2X3 receptors in DRG neurons that was associated with the neuronal hyperexcitability and the cancer-induced bone pain in rats: VILIP-1, which was first detected in DRG neurons in our experiments, interacted with P2X3 receptor C-terminus and enhanced the expression and function of the receptor, which in turn caused hyperexcitation of DRG neurons that is proposed to underlie the pathogenesis of cancer-induced bone pain. Thus, functional upregulation of P2X3 receptors by VILIP-1 in DRG neurons contributes to the development of bone cancer pain in a rat model.

2. Materials and methods

2.1. Chemicals, antibodies, and animals

α,β-meATP (Tocris Bioscience, Bristol, UK) and A-317491 (Sigma-Aldrich, St. Louis, MO) were dissolved in sterile 0.9% saline solution as a 100 mM stock solution, stored at −20°C, and diluted to desired concentrations just before experiments. Trypsin, collagenase, and poly-D-lysine were purchased from Sigma-Aldrich.

Polyclonal rabbit anti-rat P2X3 and guinea pig anti-rat P2X3 antibodies were obtained from Alomone Labs (Jerusalem, Israel) and Millipore Corp (Billerica, MA), respectively. Polyclonal rabbit anti-rat VILIP-1 antibody was from Abnova (Taipei City, Taiwan). Lectin from Bandeiraea simplicifolia BS-I isolectin B4 TRITC/FITC conjugate, mouse anti-rat FLAG, mouse anti-rat calcitonin gene related peptide (CGRP) and neurofilament, heavy polypeptide (NF200) antibodies were all from Sigma-Aldrich. Mouse anti-rat Neuronal Nuclei (NeuN) antibody was from Chemicon International (Temecula, CA). Na^+,K^+-ATPase β2 antibody was from BD Biosciences (Franklin Lakes, NJ). Monoclonal glutathione-*S*-transferase (GST) and His_6 antibodies were obtained from Applygen (Beijing, China). Monoclonal antibodies against green fluorescent protein (GFP), β-actin, glyceraldehyde 3-phosphate dehydrogenase (GAPDH), and horseradish peroxidase–labeled secondary antibodies were purchased from Santa Cruz Biotechnology (Santa Cruz, CA). Alexa Fluor 568 goat anti-mouse IgG (H+L) and Alexa Fluor 488/543 goat anti-rabbit IgG (H+L) were obtained from Invitrogen (Carlsbad, CA). All restriction enzymes were purchased from Takara Bio Inc. (Shiga, Japan), and all cell culture media were from Invitrogen.

Adult Sprague-Dawley rats weighing 180 to 220 g at the beginning of the experiments were provided by the Department of Experimental Animal Sciences, Peking University Health Science Center. The rats were housed in separated cages with free access to food and water. The room temperature was kept at 24 ± 1°C under natural light/dark cycle. All animal experimental procedures were carried out in accordance with the guidelines of the International Association for the Study of Pain [48] and were approved by the Animal Care and Use Committee of Peking University.

2.2. Plasmid construction, mutation, and transfection

wtpCDNA3.1(+)-P2X3 was kindly provided by Dr. R.A. North (Manchester University, Manchester, UK), and wtVILIP-1 was generously provided by Dr. K.-H. Braunewell (Southern Research Institute, Birmingham, AL) and Dr. F. Coussen (Institute for Interdisciplinary Neuroscience, Bordeaux, France). Empty vectors pFlag-CMV, pCDNA-His-Myc and pET-32a were a generous gift from Dr. Li Liu (Sichuan Agricultural University, Sichuan, China). All constructs were made by polymerase chain reaction (PCR) using appropriate pairs of forward and reverse synthetic oligonucleotide primers (AUGCT, Supplementary Table S6) and Taq polymerase (Takara Bio, Otsu, Shiga, Japan). VILIP-1-FLAG, VILIP-2-FLAG, VILIP-1-DsRed, and VILIP-1–green fluorescent protein (GFP) plasmids were constructed by PCR from rat brain cDNA and subcloned into the SalI–BamHI site of the pFlag-CMV and pDsRed-C1 vector (Clontech, Mountain View, CA) or the HindIII–BamHI site of the pEGFP-N1 vector (Clontech). P2X3-CFP and P2X3-His-Myc plasmids were constructed by PCR from P2X3-WT plasmid and subcloned into the BglII–EcoRI site of the pECFP-N1 (Clontech) and pCDNA-His-Myc vector. Prokaryotic expression constructs of GST-VILIP-1 full length and $GST_{\Delta 1\text{-}22}$ were generated by PCR from rat brain cDNA and subcloned into the BamHI–SalI site of the pGEX-5X-1 vector (Clontech). $GST_{\Delta 23\text{-}191}$, $GST_{\Delta 59\text{-}191}$, $GST_{\Delta 96\text{-}191}$ and $GST_{\Delta 132\text{-}191}$ were generated by PCR from rat brain cDNA and subcloned into the EcoRI–XhoI site of the pGEX-5X-1 vector. Prokaryotic expression constructs encoding P2X3 C-terminal tail were generated by PCR from pCDNA3.1(+)-P2X3 and subcloned into the EcoRI–XhoI site of the pGEX-5X-1 vector or the SalI–HindIII site of the pET-32a vector. The nonmyristoylatable mVILIP-1-myr mutant was achieved by mutagenesis of residue glycine 2 to alanine using the corresponding primers. The sequence of plasmids and mutations was confirmed by DNA sequencing (Sunbiotech, Beijing, China).

Transfections of plasmids into HEK293 cells were carried out using Lipofectamine 2000 (Invitrogen), as previously described [26]. Briefly, plasmids and transfection reagent (1.5 μL per microgram of DNA) were each diluted with Dulbecco's modified Eagle medium (DMEM), mixed together, and incubated for 20 minutes at room temperature. The mixture was then added to the medium for transfection. After 5 hours, the medium was replaced by DMEM supplemented with 10% fetal bovine serum (FBS) (HyClone, Logan, Utah, USA). Cells were used 36 to 48 hours after transfection.

2.3. Surface protein biotinylation

Cell surface biotinylation was performed in HEK293 cells transfected with plasmids as previously described by Bao et al. [1]. In brief, HEK293 cells transfected with plasmids were washed with cold phosphate-buffered saline (PBS) and then incubated in PBS containing 800 mg/mL sulfo-NHS-LC-biotin (Pierce, Rockford, Illinois, USA) for 45 minutes at 4°C to biotinylate surface proteins. After stopping the reaction with cold PBS containing 1 mM glycine, cells were lysed in buffer containing 0.1% Triton X-100, 0.1% sodium docecylsulfate (SDS), 150 mM NaCl, 10 mM Tris-HCl (pH 7.4), and protease inhibitor cocktail (Roche, Indianapolis, Indiana, USA). Cell debris was removed by centrifugation at 12,000 rpm for 10 minutes at 4°C. Two hundred micrograms of cell lysates were incubated with 30 μL immobilized NeutrAvidin agarose (Pierce) at 4°C overnight. Then, agarose pellets were washed 5 times in lysis buffer. Finally, biotinylated surface proteins were eluted from agarose beads by boiling at 95°C for 5 minutes in

SDS sample buffer. Proteins were separated by SDS-polyacrylamide gel electrophoresis (SDS-PAGE), transferred to PVDF membrane (Millipore) and blotted with antibodies against His (1:1000) together with β-actin (1:3000) antibody.

2.4. DRG neurons culture, LV infection, and immunocytochemistry

Primary culture of DRG neurons was performed according to the modified method described by Natura et al. [30]. In brief, rats (age 2 weeks) were euthanized with ether and DRGs were dissected from all spinal segments. The DRGs were digested with collagenase type IA (3 mg/mL, Sigma-Aldrich) for 45 minutes and 0.25% trypsin (Sigma-Aldrich) for another 10 minutes at 37°C. After terminating the enzymatic treatment by DMEM plus 10% FBS, ganglia were dissociated with a polished Pasteur pipette, and the suspension of ganglia was sieved through a filter to remove debris and centrifuged at 800*g* for 2 minutes. The cell pellet was resuspended in DMEM supplemented with 10% FBS. The resuspended cells were plated on 35-mm dishes coated with poly-D-lysine (0.5 mg/mL), kept for 3 hours, and replaced with Neurobasal growth medium containing B27 supplement, 0.5 mM L-Glutamax (Sigma-Aldrich), 2.5 M cytosine arabinoside (Sigma-Aldrich), 100 U/mL penicillin, and 100 g/mL streptomycin, The cells were kept at 37°C in an incubator with 5% CO_2 and 95% air. Cultures were fed daily with Neurobasal growth medium containing B27 supplement.

Recombinant lentivirus VILIP-1-green fluorescent protein (LV-VILIP-1-GFP) and LV-short hairpin (sh)VILIP-1 were constructed by Genechem (Shanghai, China). Briefly, the plasmids expressed VILIP-1-GFP or shVILIP-1-GFP was used to produce lentivirions. VILIP-1-GFP was cloned into the LV vector GV208 (Genechem, Shanghai, China), which is a lentiviral packaging vector with ubiquitin promoter. LV-short hairpin RNA (shRNA) was generated using sense small interfering RNA sequence targeting VILIP-1 (GeneBank accession number 24877): small interfering (si) VILIP-1 (303-323) GCATGAGCTCAAGCAGTGGTA. The scrambled sequence was used as negative control. To minimize off-target effects, a BLAST homology search (based on sense and antisense sequences) was systematically performed to ensure that a single mRNA sequence was targeted (http://www.ncbi.nlm.nih.gov). Lentiviral vector is GV118 (Genechem, Shanghai, China) with U6 promoter. The short hairpin RNAs were cloned into LV vectors. Construction and production of lentivirions were completed by Genechem. The final titer of recombinant virus was around 1×10^9 transducing units (TU)/mL. Cultured DRG neurons on days 5 to 7 in vitro were exposed to virus for 8 hours at a multiplicity of infection of 30. Experiments were performed 48 to 72 hours after infection.

LV-infected DRG neurons that were cultured on 35-mm dishes were rinsed for 5 minutes with PBS and fixed for 10 minutes with 4% paraformaldehyde in PBS at room temperature. After another washing for 5 minutes, neurons were blocked for 1 hour at room temperature with 10% goat serum in PBS and incubated with rabbit anti-rat P2X3 antibody (1:1000) in PBS overnight at 4°C. After 3 washes in PBS, neurons were incubated for 1 hour with appropriate secondary antibody. After another 3 washes in PBS, neurons were mounted and observed with confocal microscopy as described previously. Image acquisitions were performed on GFP-positive neurons.

2.5. Biochemical fractionation of DRG tissues by graded extraction

L4 and L5 DRGs were dissected and lysed by homogenization with Nucl-Cyto-Mem preparation kit (Applygen) according to the manufacturer's instructions with some modifications as previously described [18]. The membrane pellet was sonicated and re-extracted with buffer D containing 10 mM Tris-HCl (pH 8.0), 150 mM NaCl, 1% Triton X-100, 0.5% sodium deoxycholate, and 0.1% SDS, and then fractionated by centrifugation at 14,000 rpm at 4°C for 30 minutes, and the supernatant was labeled as SDS-soluble fraction. The pellet was dissolved by sonication and boiling in buffer E containing 3% SDS and 5% β-mercaptoethanol (1 mL/g pellet), and the lysate was termed SDS-insoluble fraction. The fractions were loaded on separate lanes, and each fraction was analyzed by immunoblot with P2X3 receptors (1:1000), glyceraldehyde 3-phosphate dehydrogenase (GADPH) (1:5000) and Na^+,K^+ ATPase (1:1000) antibodies.

2.6. Western blot

Under deep anesthesia with 10% chloral hydrate (0.3 g/kg, intraperitoneally [i.p.]), the rat L4–L5 DRGs, the dorsal horn of the spinal cord, and the cortex were removed and immediately homogenized in ice-chilled lysis buffer containing 50 mM Tris (pH 8.0), 150 mM NaCl, 1% NP40 (Sigma-Aldrich), 0.5% sodium deoxycholate (Sigma-Aldrich), 0.1% SDS, and protease inhibitor cocktail (Roche). In some experiments, the LV-infected neurons, or HEK293 cells transfected with either VILIP-1-FLAG or VILIP-2-FLAG, were also lysed with the same lysis buffer. Then, the homogenates were centrifuged at 12,000 rpm for 10 minutes at 4°C, and the supernatant was analyzed. Twenty micrograms (P2X3 receptors) or 60 μg (VILIP-1 or VILIP-2) of solubilized protein from the supernatant fraction were mixed with 4× loading buffer subjected to SDS-PAGE. Proteins were electrophoretically transferred onto a PVDF membrane. After blocking with 5% nonfat milk in Tris-buffered saline and Tween (20 mM Tris-HCl, pH 7.5, 150 mM NaCl, and 0.05% Tween-20) for 60 minutes at room temperature, the membranes were incubated with the following primary antibodies at 4°C overnight: rabbit anti-rat P2X3 antibody (1:1000, Alomone Labs), rabbit anti-rat VILIP-1 antibody (1:100, Abnova), mouse anti-FLAG antibody (1:1000, Sigma-Aldrich), mouse anti-β-actin (1:3000, Santa Cruz Biotechnology), or mouse anti-GAPDH (1:5000, Santa Cruz Biotechnology). The blots were washed in Tris-buffered saline and Tween and then incubated in horseradish peroxidase–conjugated goat anti-rabbit/mouse IgG secondary antibody (1:2000, Santa Cruz Biotechnology). Protein bands were visualized using an enhanced chemiluminescence detection kit (Pierce) followed by autoradiography using Hyperfilm MP (Santa Cruz Biotechnology). The standardized ratio of P2X3 or VILIP-1 to GAPDH (or β-actin) band density was used to calculate the alteration in P2X3 or VILIP-1 expression. For quantifying P2X3 or VILIP-1 expression, the mean values in the control group (naive) were converted to 100% (1.0) as a baseline definition, and then individual data, including the control group, were recalculated as a ratio of the mean values.

2.7. Immunohistochemistry

Deeply anesthetized rats were intracardially perfused with 50 mL of 0.1 M phosphate buffer (PB) followed by 500 mL of cold 4% paraformaldehyde (in 0.1 M PB, pH 7.4). The left L4 and L5 DRGs or the cortex were quickly removed, postfixed in the same fixative solution for 2 hours and then were cryoprotected in 30% sucrose (in 0.1 M PB). Several days later, the tissues were sectioned at 8-μm thickness for DRG sections and 30-μm thickness for cortex on a cryostat. For P2X3 receptor immunostaining, DRG sections were co-incubated with a combination of rabbit anti-rat P2X3 receptor antibody (1:1000, Alomone Labs) and rabbit anti-rat VILIP-1 (1:100, Abnova) in 1% bovine serum albumin and 0.3% Triton X-100 in 0.01 M PBS, overnight at 4°C. For VILIP-1 immunostaining, DRG or cortex sections were co-incubated with a combination of rabbit anti-rat VILIP-1 antibody and one of the following antibodies: (1) mouse anti-rat NF200; (2) IB4-TRITC; (3) mouse anti-rat CGRP; (4) mouse anti-rat NeuN (1:100, Chemicon)

as indicated solutions. After washing with PBS, sections were incubated with Alexa Fluor 488 goat anti-rabbit IgG (H+L) (1:2000, Invitrogen), Alexa Fluor 568 goat anti-mouse IgG (H+L) (1:2000, Invitrogen) or Alexa Fluor 543 goat anti-rabbit IgG (H+L) (1:2000, Invitrogen) for 1 hour at room temperature. Stained slides were viewed and photographed with a charge-coupled device camera under a fluorescent microscope (Olympus, Tokyo, Japan).

2.8. GST pull-down assay

GST- or His_6-fusion proteins were expressed in the BL21 *Escherichia coli* strain and purified according to the manufacturer's instructions. For binding assays, GST or GST-fusion protein was immobilized on glutathione-Sepharose resin (GE Healthcare, Piscataway, NJ, USA). His_6-fusion protein was purified using Ni-nitrilotriacetic acid magnetic beads (QIAGEN, Valencia, CA, USA). The protein extracts from rat DRGs, HEK293 cells transfected with VILIP-1 plasmid, or purified His_6-fusion protein were then incubated with the immobilized GST or GST-fusion protein for 3 hours at 4°C, washed, boiled, and subjected to SDS-PAGE.

2.9. Co-immunoprecipitation in vitro and in vivo

HEK293 cells transfected with plasmids or dissected rat DRGs were immediately homogenized in ice-cold lysis buffer containing 20 mM Tris-HCl (pH 7.4), 100 mM NaCl, 1% NP40, and complete protease inhibitor cocktail. After being rotated at 4°C for 1 hour, the homogenates were centrifuged at 12,000 rpm for 10 minutes to yield the total protein extract in the supernatant. Protein extracts from cell cultures or tissues were incubated with either anti-P2X3 (1:1000, Alomone Labs) or anti-FLAG antibody (1:1000, Sigma-Aldrich) at 4°C for 3 hours. Protein A/G agarose (Santa Cruz Biotechnology) was added to the samples, and the incubation was continued for another 12 hours. Subsequently, the samples were washed 6 times with lysis buffer and subjected to SDS-PAGE.

2.10. mRNA extraction and reverse-transcription PCR

Rat L4–L5 DRG or the cortex was homogenized in TRIzol (Invitrogen) reagent, and total RNA was isolated using PrimeScript RT-PCR kit (Takara Bio) according to the manufacturer's instructions. Reverse transcription was performed with 1 μg of total RNA by using several primers as indicated.

2.11. Whole-cell patch clamp recordings

Whole-cell patch clamp recordings from acutely dissociated DRG neurons or plasmids transfected HEK293 cells were performed at room temperature using an EPC-10 amplifier and Patchmaster software (HEKA, Freiburg, Germany). Patch pipettes were pulled from borosilicate glass capillaries with a tip resistance of 5 to 8 MΩ when filled with internal solution containing 140 mM K-aspartate, 20 mM NaCl, 10 mM ethylene glycol tetraacetic acid (EGTA), and 5 mM 4-(2-Hydroxyethyl) piperazine-1-ethanesulfonic acid (HEPES), adjusted to pH 7.3 with Potassium hydroxide (KOH). The external solution contained 155 mM NaCl, 5 mM KCl, 2 mM $CaCl_2$, 1 mM $MgCl_2$, 10 mM HEPES, and 12 mM glucose, adjusted to pH 7.4 with NaOH [5]. Drugs were prepared in the external solution and delivered by a gravity-fed multibarrel perfusion system (VaveLink 8; Automate Scientific, Inc., Berkeley, CA, USA). Membrane currents and voltage were measured with pipette and membrane capacitance cancellation, filtered at 2 kHz, and digitized at 10 kHz. Resting membrane potential was measured immediately after rupture of the cell membrane in whole-cell patch mode.

Under voltage-clamp recording, cells were clamped at −70 mV, and series resistance was compensated 70% to 90%. The membrane capacitance was read from the amplifier by Patchmaster software (HEKA) for determining the size of cells and calculating the current density. The agonist-evoked P2X currents were measured by application of α,β-meATP (20 μM for 3 seconds). Rise times (T_a) of α,β-meATP responses were obtained by measuring the activation time between 10% and 90% of the peak value. The time constants of current inactivation (τ_{in1} and τ_{in2}) were obtained by fitting the decay phase of the currents with exponential functions using the Levenberg-Marquardt algorithm as previously described [42]. Origin software 8.5 (OriginLab Corporation, Northampton, MA) was used for data analysis and fitting.

Under current-clamp recording, cells were held at 0 pA, and the agonist-evoked depolarization was recorded by application of α,β-meATP (20 μM for 3 seconds) to DRG neurons. The depolarization amplitude was measured by the distance between resting potential and threshold potential in discharged neurons. In some neurons, action potential discharges were elicited when the depolarization amplitude exceeded the neuronal threshold potential.

2.12. Inoculation of tumor cells

A rat model of bone cancer pain was established by intratibial injection of syngeneic MRMT-1 rat mammary gland tumor cells as previously described [28]. Briefly, after anesthetized with chloral hydrate (0.3 g/kg, i.p.), the rat left tibia was carefully exposed, and a 23-gauge needle was inserted in the intramedullary canal of the bone. It was then removed and replaced with a long, thin blunt needle attached to a 10-μL Hamilton syringe containing the medium to be injected. A volume of 4 μL MRMT-1 rat mammary gland tumor cells (4×10^4) or vehicle (PBS) was injected into the tibial bone cavity. After injection, the site was sealed with bone wax and the wound was finally closed. None of the animals showed signs of motor dysfunction after inoculation of tumor cells.

2.13. Assessment of mechanical allodynia

Mechanical allodynia, as a behavioral sign of bone cancer pain, was assessed by measuring 50% paw withdrawal threshold (PWT) as described in our previous report [16]. The 50% PWT in response to a series of von Frey filaments (Stoelting, Wood Dale, IL) was determined by the up and down method [7]. The rat was placed on a metal mesh floor covered with an inverted clear plastic cage ($18 \times 8 \times 8$ cm) and allowed a 20-minute period for habituation. Eight von Frey filaments with approximately equal logarithmic incremental (0.224) bending forces were chosen (0.41, 0.70, 1.20, 2.00, 3.63, 5.50, 8.50, and 15.10 g). Each trial started with a von Frey force of 2*g* delivered perpendicularly to the plantar surface of the left hindpaw for ~2 to 3 seconds. An abrupt withdrawal of the foot during stimulation or immediately after the removal of the hair was recorded as a positive response. Whenever there was a positive or negative response, the next weaker or stronger filament was applied, respectively. This procedure was done until 6 stimuli after the first change in response had been observed. The 50% PWT was calculated using the following formula: $50\%\ \mathrm{PWT} = 10^{[X_f + k\delta]}$, where X_f is the value of the final von Frey filament used (in log units), k is a value measured from the pattern of positive/negative responses, and $\delta = 0.224$, which is the average interval (in log units) between the von Frey filaments [13]. If an animal responded to the lowest von Frey filament, a value of 0.25*g* was assigned. If an animal did not respond to the highest von Frey filament, the value was recorded as 15.0*g*. The mechanical allodynia was assessed by measuring the 50% PWT of ipsilateral hind paw in tumor cells inoculated- or sham-operated rats. In rats, mechanical allodynia is assessed by measuring the 50% PWT to von Frey filaments, and an allodynic rat is defined as that the 50% PWT is <4.0 g (ie, withdrawal in response to non-noxious tactile stimulus) [47].

2.14. Assessment of thermal hyperalgesia

Thermal hyperalgesia of the hind paws was tested as described by our previous report [46]. Rats were allowed to acclimate for a minimum of 30 minutes within acrylic enclosures on a clear glass plate maintained at 30°C. A radiant heat source was focused onto the plantar surface of the hind paw. Measurements of paw withdrawal latency (PWL) were taken by a timer that was started by the activation of the heat source and stopped when withdrawal of the paw was detected with a photodetector. A maximal cutoff time of 30 seconds was used to prevent unnecessary tissue damage. Three measurements of PWL were taken for each hind paw and were averaged as the result of each test session. The hind paw was tested alternately with >5-minute intervals between consecutive tests.

2.15. Implantation of intrathecal catheter

Under chloral hydrate (0.3 g/kg, i.p.) anesthesia, implantation of intrathecal cannula was performed as described in our previous study [33]. Briefly, a PE-10 polyethylene catheter was implanted between the L5 and L6 vertebrae to reach the lumber enlargement of the spinal cord. The outer part of the catheter was plugged and fixed onto the skin on closure of the wound. All surgical procedures were performed under sterile conditions. Rats showing neurological deficits after the catheter implantation were euthanized. LVs were intrathecally injected via the implanted catheter in a 20-μL volume of solution followed by 10 μL of normal saline solution for flushing. Each injection lasted at least 5 minutes. After an injection, the needle remained in situ for 2 minutes before being withdrawn.

2.16. Measurement of antagonist effects on pain behaviors

To examine effects of pharmacological blockade of P2X3 receptors with selective antagonist A-317491 in bone cancer rats, A-317491 (at a dose of 3, 10, 30, and 100 nmol/rat in a 10-μL volume of solution, respectively) was intrathecally delivered on day 14 after inoculation of tumor cells when cancer pain behaviors appeared (as confirmed by measuring mechanical allodynia and thermal hyperalgesia) [46]. Pain behaviors of mechanical allodynia and thermal hyperalgesia were measured at 2, 4, and 24 hours after drug injection, respectively.

2.17. Intrathecal delivery of lentivirions: expression, function, and behavior assays

Lentivirions including LV-VILIP-1, LV-shVILIP-1, and the control LV-GFP were intrathecally delivered at the final titer of 1×10^9 TU/mL in a 10-μL volume of solution, respectively. In some experiments such as overexpression or knockdown of VILIP-1 in naive rats, the lentivirions were intrathecally applied on day 5 after intrathecal catheter implantation. In other experiments such as knockdown of VILIP-1 by pre- or post-treatment with LV-shVILIP-1 in MRMT-1 rats, the lentivirions of shVILIP-1 or their control LV-GFP were intrathecally administrated on day 7 or 11 after MRMT-1 tumor cell inoculation, respectively.

At 7 to 14 days after lentivirion injection, expression of LV-VILIP-1 or LV-shVILIP-1 on DRG neurons was directly observed by GFP fluorescence; on the other hand, the expression of P2X3 receptors and endogenous VILIP-1 in DRG lysates was examined by Western blot; meanwhile, the α,β-meATP– (20 μM, for 3 seconds) evoked fast-inactivating P2X3 currents and the neuronal depolarization were measured by whole-cell patch clamp recording from acutely dissociated IB4-positive DRG neurons. In some experiments in MRMT-1 rats, pain behaviors including mechanical allodynia and thermal hyperalgesia were tested on days 10, 14, 16, 18, and 20 after inoculation of MRMT-1 tumor cells.

2.18. Statistical analysis

Statistical analyses were performed with GraphPad Prism 5 for Windows (GraphPad Software, Inc., La Jolla, CA). All data were expressed as mean ± SEM. A 2-tailed Student *t* test was used for the comparison of the mean values between 2 groups. One-way analysis of variance (ANOVA) followed by Dunnett's multiple comparison test or 2-way ANOVA followed by the Bonferroni post hoc test was used for multiple comparison. Differences with $P < .05$ were considered statistically significant.

3. Results

3.1. Functional upregulation of P2X3 receptors in MRMT-1 rat DRGs

P2X3 receptors are selectively expressed on primary afferent nociceptors and have been implicated in modulating nociception in different models of pathological pain [4,6,19,38]. P2X3 receptors in DRG neurons are upregulated in inflammation [42], whereas nerve injury produces divergent changes in mRNA and protein expression of the receptors (eg, upregulation in uninjured and downregulation in injured afferents) [23,24,37], and increased translocation from cytoplasm to the membrane in injured neurons [9]. In this study, we first determined whether the expression of P2X3 receptors was altered in cancer rat DRGs. Using Western blot detection, we found that the total P2X3 receptor expression in ipsilateral L4 and L5 DRGs increased markedly from day 14 (161.9 ± 17.3% of sham) to day 28 (150.3 ± 11.9% of sham) in MRMT-1 rats as compared with sham rats ($P < .05$, 2-way ANOVA, n = 7) (Fig. 1A). Accordingly, a significant increase in membrane P2X3 receptor expression was also detected in SDS-soluble fraction of DRGs on day 14 in MRMT-1 rats compared with naive rats (168.1 ± 15.9% of control, $P < .01$, 1-way ANOVA, n = 3) (Fig. 1B).

To further investigate the functional alteration of P2X3 receptors in nociceptive DRG neurons in bone cancer rats, we examined the agonist (α,β-meATP)–evoked P2X currents using whole-cell patch clamp recording on IB4-labled small DRG neurons. The FITC-labeled lectin IB4 was used in initial experiments as a live cell marker to identify putative P2X3 receptor-expressing nociceptive neurons [5]. Somata of small DRG neurons were defined by their diameters (⩽30 μm) and membrane capacitance (C_m ⩽28.3 pF), as described in previous study [17]. In agreement with previous findings [5,32], we observed 2 main types of P2X currents, fast- and slow-inactivating current, on IB4-labled small DRG neurons in the presence of α,β-meATP (20 μM for 3 seconds) at a holding potential of −70 mV; of these, the majority (>50%) were fast-inactivating currents (Supplemental Figure S1 and Supplemental Table S1). It has been documented that the fast-inactivating currents were predominantly detected in small-diameter, IB4-positive, and capsaicin-sensitive DRG neurons and were found to be mediated by homomeric P2X3 receptors [32,38]. Thus, we only studied the fast-inactivating P2X3 currents on IB4-labled small DRG neurons in all of the functional experiments in this study. We found a marked increase in the current density (pA/pF) of agonist (α,β-meATP)–evoked fast-inactivating P2X3 currents in MRMT-1 rats compared with control rats (43.1 ± 4.2 MRMT-1 vs 23.6 ± 3.1 naive and 27.7 ± 4.2 sham, respectively, $P < .001$ vs naive, $P < .05$ vs sham, 1-way ANOVA, n = 20 naive, 15 sham, and 23 MRMT-1) (Fig. 1C). However, no significant alteration was observed either on the affinity to agonist (ie, the EC_{50} for activation of P2X3 receptors by agonist, Supplemental Figure S2) or on the kinetics of agonist-evoked fast P2X3 currents (ie, rise time; decay

time constant τ) (Supplemental Table S2) in MRMT-1 rats. Together with the aforementioned data on P2X3 receptor expression, we suggested that the potentiation of the P2X3 current density was likely due to the increase in P2X3 receptor expression in cancer rat DRG neurons.

Furthermore, we found that the mean depolarization amplitude induced by α,β-meATP was significantly increased in IB4-positive DRG neurons in MRMT-1 rats (22.9 ± 1.5 mV) compared with control rats (15.1 ± 0.9 mV naive, 15.8 ± 1.4 mV sham, $P < .001$, 1-way ANOVA, n = 21 naive, 22 sham, and 20 MRMT-1) (Fig. 1D). In both

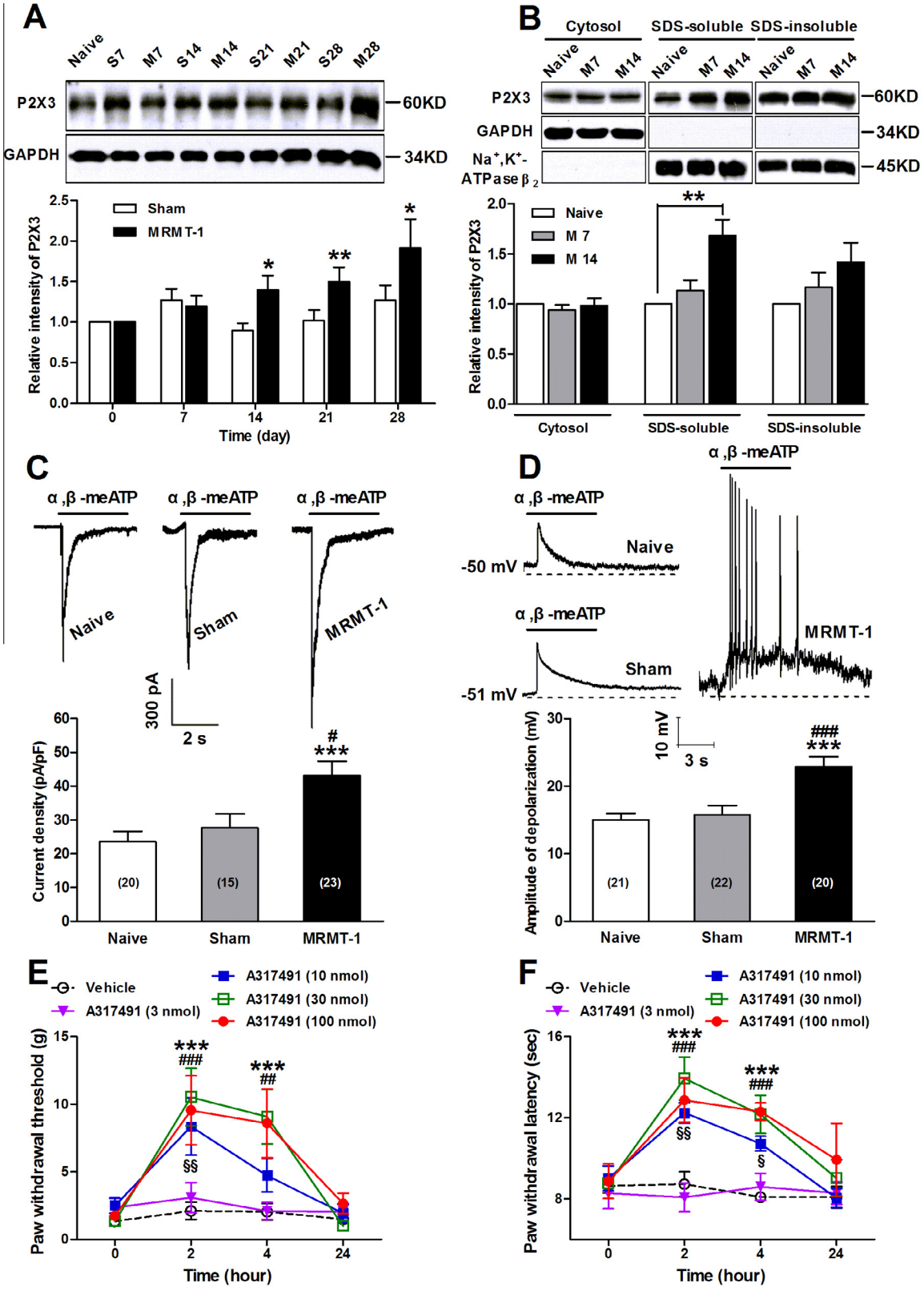

naive and sham rat DRG neurons, most of the depolarizations were subthreshold, whereas in cancer rat DRG neurons, ~50% of the depolarization was great enough to evoke action potentials (Fig. 1D, Supplemental Table S3). Unexpectedly, no alteration was observed on the resting membrane potential of DRG neurons in MRMT-1 rats (data not shown). These results suggested that the potentiation of α,β-meATP–evoked P2X3 currents likely mediated the hyperexcitability of MRMT-1 rat DRG neurons that is proposed to underlie the pathogenesis of cancer-induced bone pain [46]. In support, we found that pharmacological blockade of P2X3 receptors with selective antagonist A-317491 (at doses of 10, 30, and 100 nmol/rat) could dramatically attenuate the cancer-induced mechanical allodynia and thermal hyperalgesia as assessed respectively by PWT to von Frey filaments (10.5 ± 2.1g vs 2.1 ± 0.6g at 2 h, A-317491 30 nmol vs vehicle, $P < .001$, 2-way ANOVA, n = 6/group) (Fig. 1E) and PWL to radiant heat (13.9 ± 1.1 seconds vs 8.7 ± 0.6 seconds at 2 hours, A-317491 30 nmol vs vehicle, $P < .001$, 2-way ANOVA, n = 6–8/group) (Fig. 1F). Taken together, these data indicate that the functional upregulation of P2X3 receptors mediates the hyperexcitability of MRMT-1 rat DRG neurons, which in turn contribute to the development of cancer-induced bone pain.

3.2. Expression of VILIP-1 was detected in DRG neurons in naive rats and increased in MRMT-1 rats

To further elucidate the mechanisms underlying the functional upregulation of P2X3 receptors in bone cancer rats, we focused on VILIP-1, a neuronal calcium sensor protein that has been proposed to potentially function as a general regulator of ligand-gated ion channels [3,8]. We first determined whether VILIP-1 was expressed on naive rat DRG neurons, which have not been reported in previous studies. Using antibody against VILIP-1 (1:100, Abnova), we did detect the expression of VILIP-1 on naive rat DRG neurons (Fig. 2A, a) and as a positive control also on the cortex cells (Fig. 2A, b). Moreover, double immunofluorescence staining showed that the expression of VILIP-1 was universally colocalized with NeuN-, IB4-, CGRP-, and NF200-positive DRG neurons (Fig. 2A, c–f). Using primer pairs for full-length VILIP-1, the reverse transcription PCR analysis further confirmed the expression of VILIP-1 mRNA in both DRGs and the cortex in naive rats (Fig. 2B). In addition, Western blot analysis showed that the VILIP-1 protein was detected in the dorsal horn of the spinal cord and in DRG lysates, and as a positive control, was also detected in the cortex in naive rats. Subcellular fractionation from DRG lysates showed that the VILIP-1 protein was located in both cytosolic and membrane fractions, especially in cytosolic, as the protein loading weight in membrane fraction is 6 times that in cytosol fraction (Fig. 2C). Considering the high homology between VILIP-1 and VILIP-2, we investigated whether the polyclonal VILIP-1 antibody used in our experiment has the possibility of cross-reactivity to VILIP-2. In HEK293 cells transfected with either VILIP-1-FLAG or VILIP-2-FLAG, parallel Western blot experiments on HEK293 cells lysates were performed using anti-FLAG (1:1000, Sigma) or anti-VILIP-1 (1:100, Abnova) antibody. The results showed that the anti-FLAG antibody reacted with both VILIP-1-FLAG and VILIP-2-FLAG, whereas the anti-VILIP-1 at a 1:100 dilution only reacted with VILIP-1-FLAG (Supplemental Figure S3). These data suggested that the polyclonal VILIP-1 antibody used in our experiment had no cross-reactivity to VILIP-2.

Next, we examined the alterations of VILIP-1 in MRMT-1 rat DRGs. Western blot revealed that the expression of VILIP-1 protein was dramatically enhanced from day 14 (223.3 ± 41.7% of sham, $P < .01$, 2-way ANOVA, n = 5) to day 28 (322.7 ± 69.2% of sham, $P < .001$, 2-way ANOVA, n = 5) after inoculation of tumor cells (Fig. 2D), which approximately paralleled the upregulation of P2X3 receptors on the time line (Fig. 2E). Correlation analysis showed that the alterations of P2X3 receptors and VILIP-1 had a significant positive correlativity ($r^2 = 0.384$, $P = .0016$, n = 5) (Fig. 2F).

3.3. Interaction between VILIP-1 and P2X3 receptors

To determine whether VILIP-1 interacted with P2X3 receptors, as it was shown to form a signaling complex with P2X2 receptors in previous studies [8], we first performed co-immunoprecipitation experiments in HEK293 cells transfected with various plasmids including P2X3, VILIP-1, P2X3-ECFP, and VILIP-1-FLAG as indicated in Figs. 3A and 3B. Using antibody against either P2X3 receptors or FLAG for immunoprecipitation, we found that VILIP-1 was definitely bound to P2X3 receptors (Figs. 3A and 3B). Next, to verify the interaction between VILIP-1 and P2X3 receptor, GST pull-down assays were performed using the P2X3 receptor C-terminal tail (P2X3CT) as bait protein. Purified P2X3CT protein was incubated with VILIP-1 expressed in HEK293 cells. As shown in Fig. 3C, VILIP-1 was found to bind to the bacterially expressed GST-P2X3CT fusion protein but not to GST alone, implying interaction between VILIP-1 and the C-terminal tail of P2X3 receptors. To further confirm the association of endogenous VILIP-1 and P2X3 receptors, double immunofluorescence staining was carried out in naive rat DRG neurons. We found that VILIP-1 colocalized with P2X3 receptors in most DRG neurons (Fig. 3D). Moreover, similar interaction between VILIP-1 and P2X3 receptors was further validated in rat DRG lysates using antibody against P2X3 receptors for immunoprecipitation (Fig. 3E). Finally, to identify the potential binding site for the interaction between VILIP-1 and P2X3 receptors, we constructed the nested deletions of VILIP-1 as an annotated structure in UniProtKB database (Fig. 3F). Both in vitro and one-half in vitro GST pull-down assays revealed that only deletion of the N-terminal of 1–22 amino acid (NT1–22 aa) domain in VILIP-1 blocked its

Fig. 1. Functional upregulation of P2X3 receptors in cancer rat dorsal root ganglions (DRGs). (A, B) Western blot of P2X3 receptor expression in ipsilateral L4 and L5 DRGs. Upper: Representative of Western blot bands; lower: analysis of the relative intensity of P2X3 receptors. Glyceraldehyde 3-phosphate dehydrogenase (GAPDH) and Na^+, K^+-ATPase β2 were used as internal control. Note that the expression of total P2X3 receptor protein increased markedly from day 14 to day 28 in MRMT-1 rats compared with sham rats (A), $^*P < 0.05$, $^{**}P < .01$, 2-way analysis of variance (ANOVA), n = 7/group. Similarly, the enhancement of membrane P2X3 receptor expression was also detected in sodium docecylsulfate (SDS)-soluble fraction of DRGs on day 14 in MRMT-1 rats compared with naive rats (B), $^{**}P < .01$, 1-way ANOVA, n = 3/group. (C) Agonist (α,β-meATP) evoked fast-inactivating P2X3 currents in IB4(+) DRG neurons. Upper: Representative currents evoked by application of α,β-meATP (20 μM for 3 seconds) to IB4(+)-DRG neurons in naive, sham, and MRMT-1 rats, respectively. Lower: Summary of the current density (pA/pF) of agonist-evoked P2X3 currents. Note that the α,β-meATP–evoked P2X3 currents were significantly enhanced in MRMT-1 rat DRG neurons, $^*P < .05$, $^{***}P < .001$, in contrast to naive rats, 1-way ANOVA. (D) α,β-meATP–induced depolarization in IB4(+) DRG neurons. Upper: Representative of α,β-meATP–induced depolarization in naive, sham, and MRMT-1 rat DRG neurons. Note that α,β-meATP evoked greater depolarization and action potential firing in MRMT-1 rat DRG neurons, indicating the enhancement of DRG neuron excitability in bone cancer rats. Lower: Summary of the mean depolarization amplitude induced by application of α,β-meATP to IB4(+) DRG neurons. $^{***}P < .001$, in contrast to naive rats; $^{\#\#\#}P < .001$, in contrast to sham rats, 1-way ANOVA. Numbers of recorded cells in each group were given in parentheses in each column of the panel. (E, F) Effects of intrathecal administration of A-317491, a selective P2X3 and P2X2/3 receptor antagonist, on mechanical allodynia and thermal hyperalgesia in bone cancer rats. A-317491 (at doses of 10, 30, and 100 nmol/rat) dramatically alleviated the bone cancer–induced mechanical allodynia and thermal hyperalgesia as measured by paw withdrawal threshold (E) and paw withdrawal latency (F) in MRMT-1 rats. $^{\S}P < .05$ (10 nmol), $^{\S\S}P < .01$ (10 nmol), $^{***}P < .001$ (30 nmol), $^{\#\#}P < .01$ (100 nmol), $^{\#\#\#}P < .001$ (100 nmol) compared with vehicle group, 2-way ANOVA, n = 6–8/group.

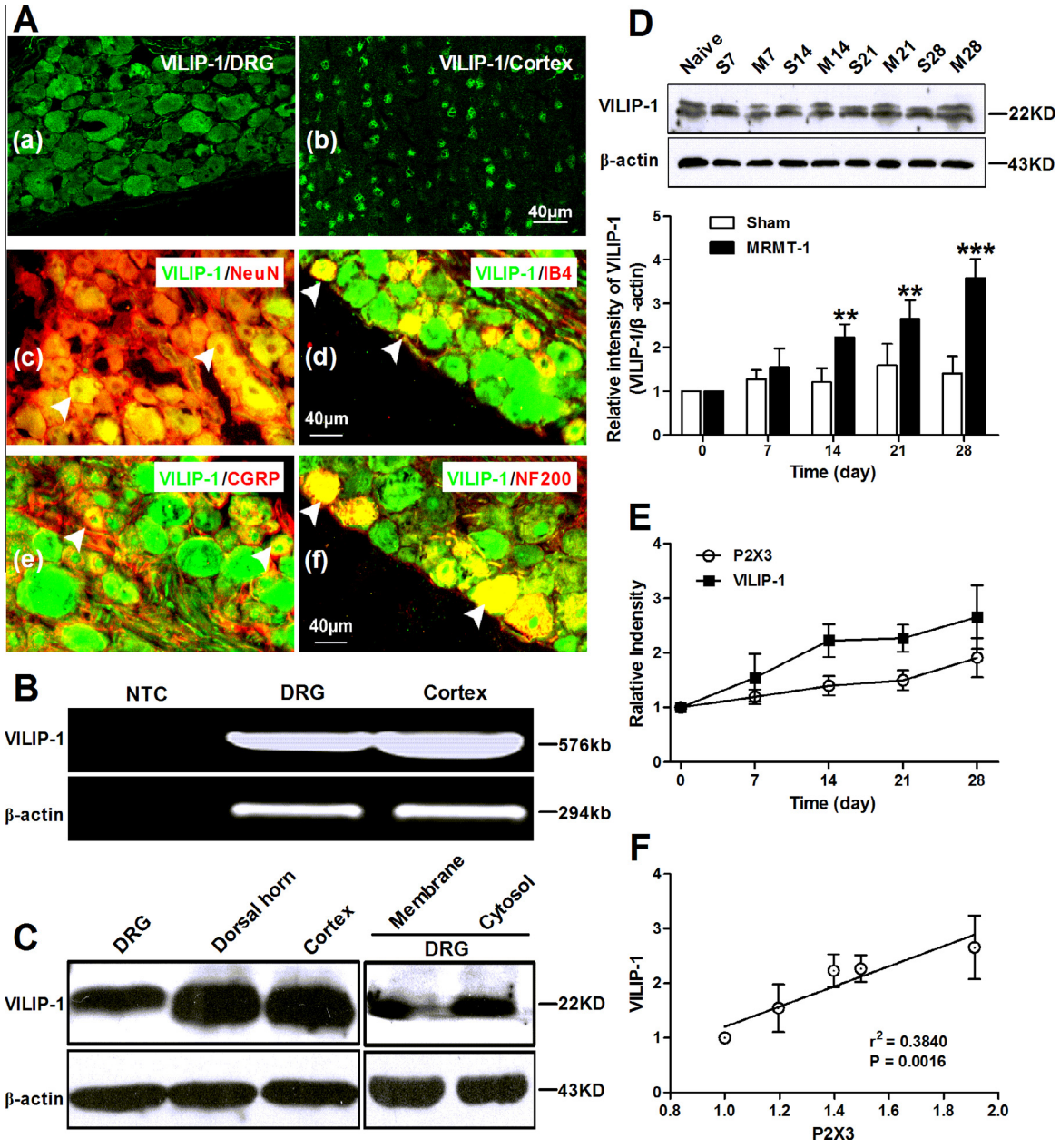

Fig. 2. Detection of visinin-like protein 1 (VILIP-1) in naive and MRMT-1 rat dorsal root ganglions (DRGs). (A) Immunohistochemical staining of VILIP-1 in naive rat DRGs. Expression of VILIP-1 was detected in DRG neurons (a), and, as a positive control, was also detected in the cortex (b). Scale bar = 100 μm, n = 3. Double immunofluorescence staining showed that the expression of VILIP-1 was colocalized with NeuN- (c), IB4- (d), calcitonin gene-related peptide- (CGRP) (e), and NF200- (f) positive DRG neurons (arrows). Scale bar = 40 μm, n = 3. (B) Reverse transcription polymerase chain reaction of VILIP-1 mRNA expression in naive rat DRGs. The expression of VILIP-1 mRNA was detected both in DRGs and in the cortex (positive control); negative control (NTC) was processed without the addition of template (n = 3). (C) Western blot analysis of VILIP-1 protein expression in naive rat DRGs. Expression of VILIP-1 protein was detected both in DRG lysates and in the spinal cord dorsal horn (the cortex was used as a positive control). Subcellular fractionation from DRG lysates showed that VILIP-1 was located in both cytosolic and membrane fractions (n = 3). (D) Expression of VILIP-1 in MRMT-1 rat DRGs. Western blot analysis showed that the expression of VILIP-1 enhanced dramatically from day 14 to day 28 after tumor cells inoculation, $^{**}P < 0.01$, $^{***}P < .001$, compared with sham rats, 2-way analysis of variance, n = 5/group. Representative of Western blot bands was inserted in the plot. S7–S28: day 7–day 28 in sham rats; M7–M28: day 7–day 28 in MRMT-1 rats. (E, F) Comparison of P2X3 receptors and VILIP-1 expression in the time line after tumor cells inoculation in MRMT-1 rats. Data on P2X3 receptor expression were obtained from Fig. 1A. Note that the upregulation of P2X3 receptors and VILIP-1 was approximately parallel in the time line after inoculation of tumor cells (E). Correlation analysis showed that the alterations of P2X3 receptors and VILIP-1 had a significant positive correlativity (F), $r^2 = 0.384$, $P = .0016$, n = 5.

binding to both the His_6-P2X3 C-terminal (Fig. 3G, top) and the endogenous P2X3 subunits in rat DRG lysates (Fig. 3G, middle), indicating that the NT1–22 aa domain containing *N*-myristoyl glycine2 in VILIP-1 likely acted as the binding sites for P2X3 receptors. Therefore, VILIP-1 interacts with P2X3 receptors in vitro and in vivo, and the NT1–22 aa domain of VILIP-1 is required for their interaction.

3.4. VILIP-1 enhances the expression and function of P2X3 receptors in HEK293 cells

Interaction of VILIP-1 with α4β2 nAChRs or P2X2 receptor enhances their surface expression and function [8,27,44]. To study whether VILIP-1 contributes to the functional upregulation of P2X3 receptors, we examined the effects of VILIP-1 on expression

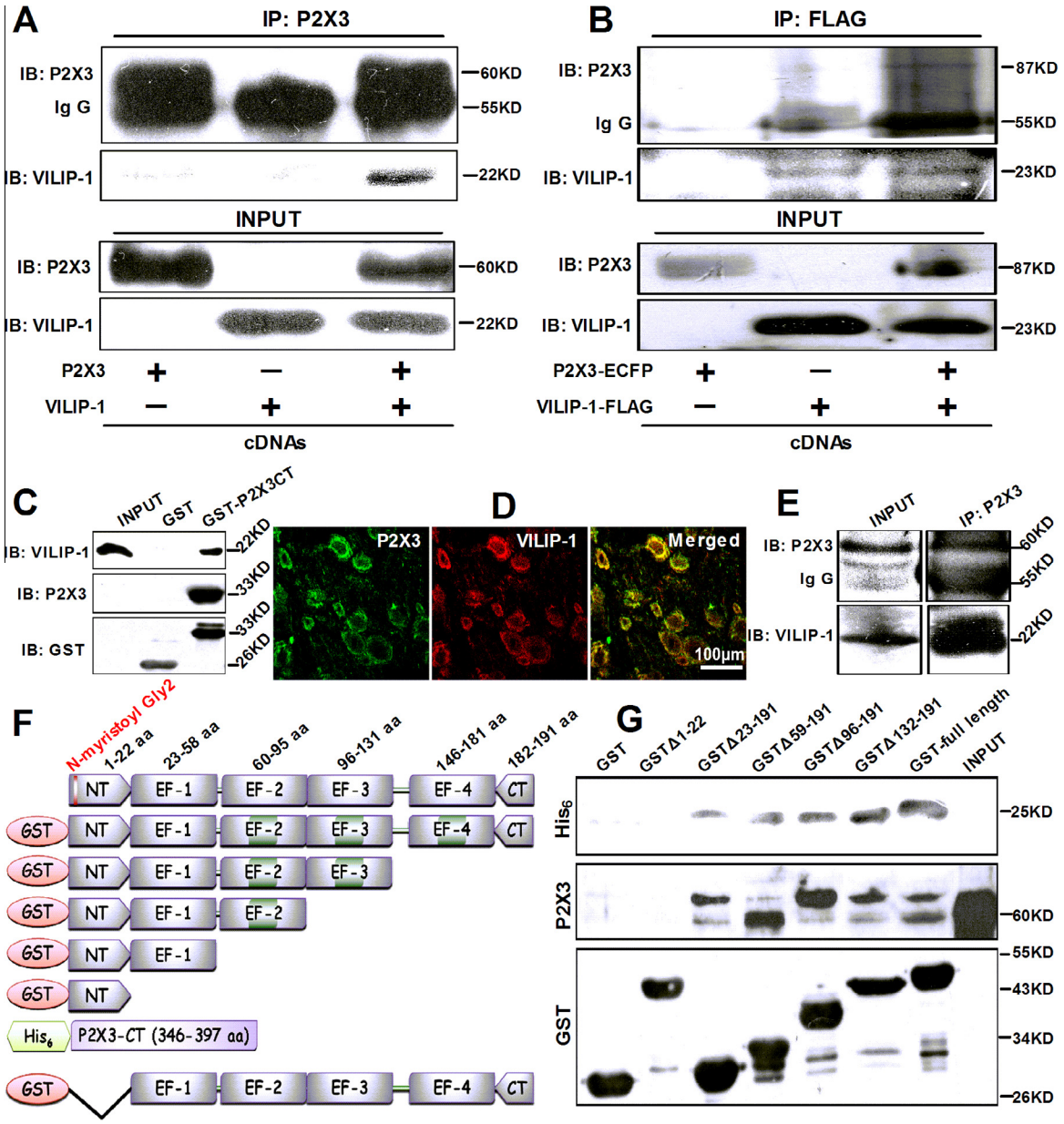

Fig. 3. Identification of the interaction between visinin-like protein 1 (VILIP-1) and P2X3 receptors in HEK293 cells and rat dorsal root ganglion (DRG) neurons. (A, B) Co-immunoprecipitation (Co-IP) of VILIP-1 with P2X3 receptors in HEK293 cells. P2X3, VILIP-1, or P2X3-ECFP and VILIP-1-FLAG were respectively transfected into HEK293 cells as indicated, and cell lysates were immunoprecipitated using anti-P2X3 (A) or anti-FLAG (B) antibody. The immunoprecipitates were examined by Western blot using anti-VILIP-1 or anti-P2X3 antibody. Co-IP revealed the association between these 2 proteins both in P2X3 and VILIP-1 and in P2X3-ECFP and VILIP-1-FLAG coexpressing HEK293 cells (n = 3). (C) Glutathione-*S*-transferase (GST) pull-down assay for the interaction between VILIP-1 and the P2X3 receptor C-terminal tail (P2X3CT) in P2X3-EGFP and VILIP-1-DsRed coexpressing HEK293 cells. GST-P2X3CT or GST control protein was incubated with VILIP-1–expressed HEK293 cells. Bounding proteins were immunoblotted with anti-VILIP-1 antibody (lane 1). The bands detected using anti-P2X3 (lane 2) and anti-GST (lane 3) antibody represented the loading amount. Note that the interaction between VILIP-1 and P2X3CT was detected (n = 3). (D) Double immunofluorescence staining of VILIP-1 with P2X3 receptors in rat DRGs. Note VILIP-1 colocalized with P2X3 receptors in most DRG neurons (n = 3). Scale bar = 100 μm. (E) Co-IP of VILIP-1 with P2X3 receptors in rat DRGs. DRG lysates were immunoprecipitated with anti-P2X3 antibody. Anti-VILIP-1 antibody was used for Western blot of immunoprecipitates. Note that Co-IP of VILIP-1 and P2X3 receptors was detected in rat DRGs (n = 3). (F) Schematic representation for the construction of mutated plasmids of GST- and His_6-fusion proteins containing different domains of VILIP-1 from UniProtKB (P62762). NT, N-terminal; CT, C-terminal. (G): Identification of the binding sites between P2X3 receptors and VILIP-1 in rat DRGs. Note $GST_{\Delta 132\text{-}191}$, $GST_{\Delta 96\text{-}191}$, $GST_{\Delta 59\text{-}191}$, $GST_{\Delta 23\text{-}191}$ and GST-full-length of VILIP-1 precipitated both His_6-P2X3CT (top) and endogenous P2X3 subunits (middle) presented in rat DRGs, whereas GST and $GST_{\Delta 1\text{-}22}$ did not, indicating that the N-terminal of 1–22 amino acid (NT1-22 aa) domain containing N-myristoyl glycine2 in VILIP-1 likely acts as the binding sites for P2X3 receptors (n = 3). The bands detected using antibody against GST represented the loading amount (bottom). "INPUT" indicates a fraction (10%) of DRG lysates used in immunoprecipitation.

and function of P2X3 receptors in HEK293 cells coexpressed P2X3-His-Myc together with VILIP-1-DsRed or a mutant, mVILIP-DsRed-myr. Considering that myristoylation of VILIP-1 at glycine2 is required for its association with the α4β2 AChRs [27,43,44] and that the NT1–22 aa domain containing *N*-myristoyl glycine2 in VILIP-1 is necessary for VILIP-1-P2X3 receptor interaction (Fig. 3G), we therefore generated a mutant, mVILIP-1-myr, that was not myristoylated because the residue where it would have been myristoylated (glycine2) was mutated to alanine. Using cell surface biotinylation analysis, we found that coexpression of VILIP-1 with P2X3 receptors upregulated both the total (116.5 ± 9.4% of control, $P < .01$, 1-way ANOVA, n = 4) and membrane (234.3 ± 21.1% of control, $P < .01$, 1-way ANOVA, n = 3) expression of P2X3 receptors compared with control cells, whereas coexpression of

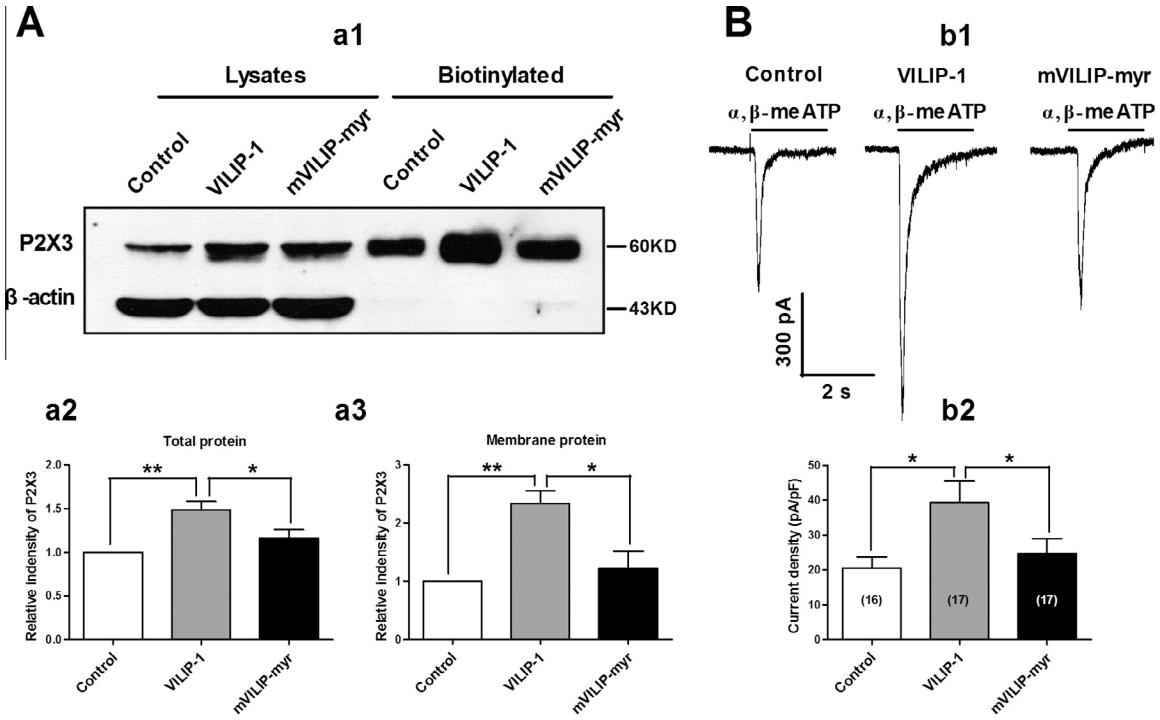

Fig. 4. Modulation of P2X3 receptors by visinin-like protein 1 (VILIP-1) in HEK293 cells coexpressed P2X3-His-Myc (P2X3) together with VILIP-1-DsRed (VILIP-1) or mVILIP-DsRed-myr (a mutated VILIP-1). (A) Western blot of P2X3 receptor expression. (a1): Representative of Western blot bands using anti-His (P2X3) and anti-β-actin antibody in cell lysates and in membrane protein biotinylation, respectively. β-Actin was used as internal control. (a2, a3): Analysis of the relative optical band density for P2X3 receptors. Note both total (a2) and membrane (a3) P2X3 receptors increased significantly in HEK293 cells coexpressed P2X3-His-Myc together with VILIP-1-DsRed (VILIP-1) compared with control (DsRed) or with mVILIP-DsRed-myr (mVILIP-1-myr), $^{*}P < .05$, $^{**}P < .01$, 1-way analysis of variance (ANOVA), n = 4/group. mVILIP-DsRed-myr (mVILIP-1-myr) is nonmyristoylatable mutant in which the *N*-myristoyl glycine2 was replaced by alanine. (B) Electrophysiological assay of P2X3 receptor function using whole-cell patch clamp recording. (b1) Representative of α,β-meATP- (20 μM for 3 seconds) evoked fast P2X3 currents in transfected HEK293 cells. (b2) Summary of the current density (pA/pF) of all recorded cells. Note that the current density enhanced markedly in HEK293 cells coexpressed P2X3 together with VILIP-1 compared with control (DsRed) or mVILIP-1-myr, $^{*}P < .05$, 1-way ANOVA, the numbers of recorded cells in each group are given in parentheses in each column of the panel.

mVILIP-1-myr had no such effects (Fig. 4A). Furthermore, using whole-cell patch clamp recording, we observed that coexpression of VILIP-1, but not mVILIP-1-myr, with P2X3 receptors significantly potentiated the current density (pA/pF) of P2X3 receptors (39.4 ± 6.1 VILIP-1 vs 20.6 ± 3.2 control, 24.7 ± 4.3 mVILIP-1-myr, $P < .05$, 1-way ANOVA, n = 16 control, 17 VILIP-1 and 17 mVILIP-1-myr) (Fig. 4B). These results suggested that VILIP-1 upregulated the expression and function of P2X3 receptors in HEK293 cells, and it appeared that myristoylation of VILIP-1 at glycine2 was required for functional upregulation of P2X3 receptors by VILIP-1.

3.5. Overexpression of VILIP-1 increases the expression and function of P2X3 receptors and enhances the neuronal excitability in rat DRG neurons

To further confirm the modulation of P2X3 receptors through VILIP-1, we investigated whether overexpression of VILIP-1 affected the functional upregulation of P2X3 receptors and the neuronal excitability both in cultured rat DRG neurons infected with LV-VILIP-1-EGFP (LV-VILIP-1) and in dissociated DRG neurons from rats receiving intrathecal delivery of LV-VILIP-1 to infect DRG neurons. We first generated LV expressing VILIP-1 linked with EGFP (LV-VILIP-1). Overexpression of VILIP-1 in cultured DRG neurons was accomplished by viral infection of LV-VILIP-1 for 48 hours. A transduction efficiency of 60% to 70% was routinely achieved as observed under fluorescence microscopy (Supplemental Fig. S4A). Using Western blot analysis, the overexpressed VILIP-1-EGFP (at 49 kDa) was detected with both anti-GFP and anti-VILIP-1 antibody (Figs. 5A and 5B). We then tested the expression of P2X3 receptors in infected DRG neurons using both immunostaining and Western blot. We found that overexpression of VILIP-1 in cells infected with LV-VILIP-1 caused an obvious increase in the immunofluorescence intensity of P2X3 receptors (Fig. 5C). Similarly, Western blot analysis revealed that the expression of P2X3 receptors increased dramatically in LV-VILIP-1 infected DRGs in contrast to naive or LV-GFP infected DRGs (166.1 ± 22.7% of naive, 183.4 ± 37.6% of LV-GFP, $P < .01$, 1-way ANOVA, n = 4/group), whereas no significant alteration was observed on endogenous VILIP-1 (Fig. 5D).

Furthermore, we set up overexpression of VILIP-1 in rat DRG neurons in vivo by intrathecal delivery of LV-VILIP-1 as described in previous studies [36]. The infected DRG neurons could be detected on day 7 after intrathecal delivery of LV-VILIP-1-EGFP or LV-GFP to rats (Supplemental Fig. S4B). Using Western blot analysis, we also found a prominent increase in expression of the P2X3 receptors in LV-VILIP-1 infected DRGs compared with naive or LV-GFP controls (168.3 ± 19.8% of naive, $P < .01$; 160.5 ± 8.2% of LV-GFP, $P < .05$, 1-way ANOVA, n = 3/group) (Fig. 5E). In addition, using whole-cell patch clamp recording on IB4-positive DRG neurons, we found that overexpression of VILIP-1 via LV-VILIP-1 infection significantly enhanced the α,β-meATP–evoked P2X3 currents (pA/PF) in contrast to naive or LV-GFP infected rats (44.4 ± 5.6 LV-VILIP-1 vs 26.2 ± 3.9 naive and 27.5 ± 3.3 LV-GFP, $P < .01$, LV-VILIP-1 vs naive; $P < .05$, LV-VILIP-1 vs LV-GFP, 1-way ANOVA, n = 21 naive, 16 LV-GFP and 21 LV-VILIP-1) (Fig. 5F). Moreover, the mean depolarization amplitude induced by α,β-meATP was obviously increased in LV-VILIP-1 infected DRG neurons (20.6 ± 1.3 mV) compared with naive (15.1 ± 0.9 mV, $P < .01$, 1-way ANOVA, n = 21) or LV-GFP infected neurons (15.0 ± 1.3 mV, $P < .01$, 1-way ANOVA, n = 21)

(Figs. 5G and 5H); among them, ~50% of the depolarization was large enough to evoke action potentials in LV-VILIP-1–infected DRG neurons (Fig. 5G, Supplemental Table S4). These results indicated that overexpression of VILIP-1 functionally upregulated the P2X3 receptors and increased the excitability of DRG neurons, which is associated with the development of bone cancer pain.

3.6. Knockdown of VILIP-1 reduces the expression and function of P2X3 receptors in rat DRG neurons

On the other hand, we also investigated whether knockdown of VILIP-1 functionally downregulated the P2X3 receptors in rat DRG neurons. We first constructed LV-expressing short hairpin RNAs

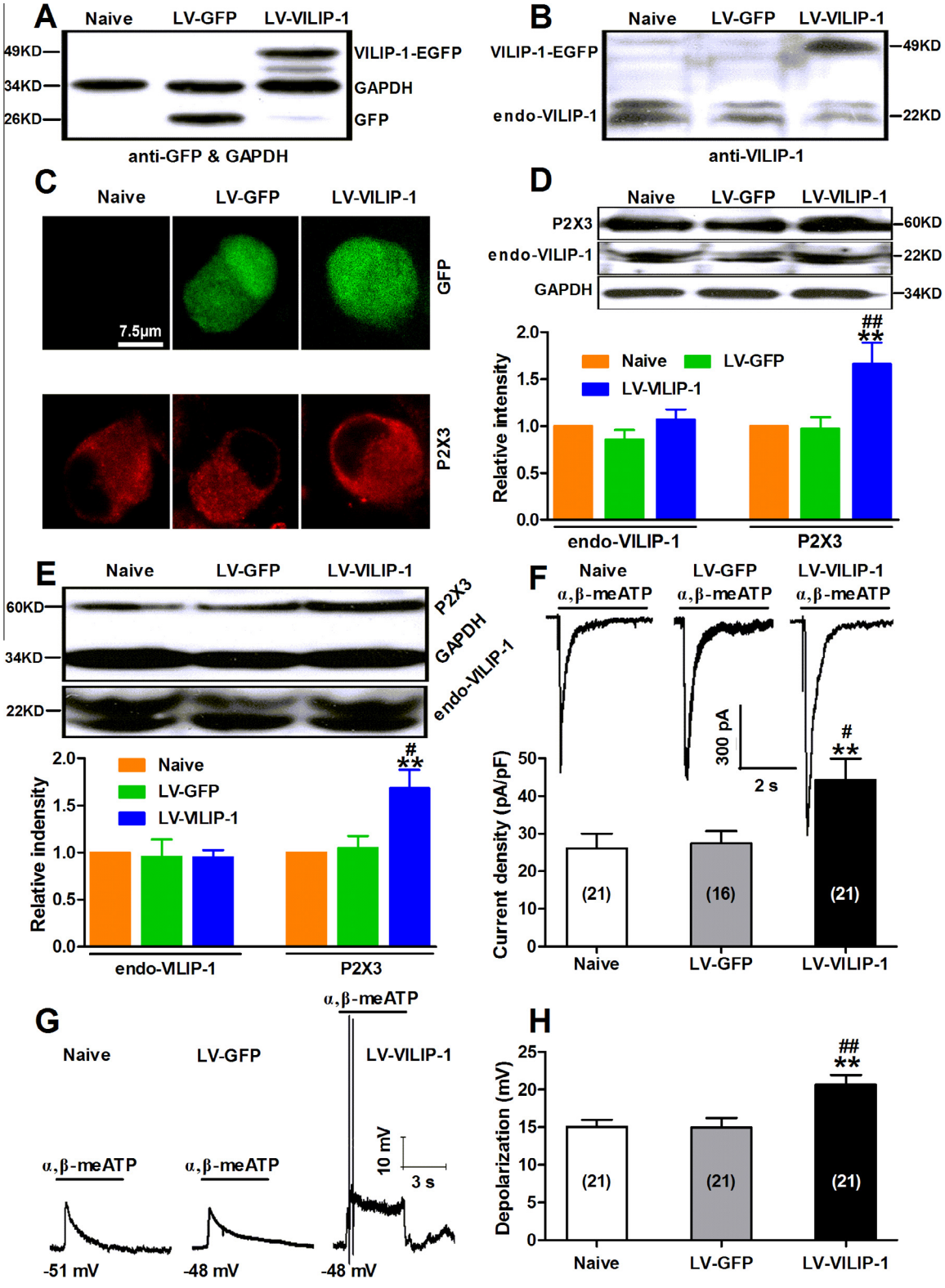

against rat VILIP-1 (LV-shVILIP-1) and LV-GFP (control). Assessment of VILIP-1 knockdown was performed in HEK293 cells coexpressed shVILIP-1 together with VILIP-1-DsRed or control plasmids. As shown in Figs. 6A and 6B, shVILIP-1 could efficiently knock down the expression of VILIP-1 in transfected HEK293 cells (32.6 ± 8.2% of control at 1.0 μg and 22.9 ± 4.0% of control at 2.0 μg, respectively, $P < .001$, 1-way ANOVA, n = 3/group). Then, knockdown of VILIP-1 in cultured DRG neurons was carried out by viral infection of LV-shVILIP-1 for 48 hours as described previously. A transduction efficiency of 80% to 90% was routinely achieved as observed under fluorescence microscopy (Supplementary Fig. S5A). The expression of P2X3 receptors in infected DRG neurons was examined using both immunostaining and Western blot. We found that the immunofluorescence intensity of P2X3 receptors decreased significantly in LV-shVILIP-1–infected DRG neurons in contrast to naive or LV-GFP–infected DRG neurons (Fig. 6C). Similarly, Western blot analysis showed that knockdown of endogenous VILIP-1 caused significant downregulation of P2X3 receptor expression (57.6 ± 4.7% of naive, $P < .01$; 54.3 ± 3.6% of LV-GFP, $P < .001$, 1-way ANOVA, n = 4/group) (Fig. 6D).

Furthermore, we set up knockdown of VILIP-1 in rat DRG neurons in vivo by intrathecal delivery of LV-shVILIP-1 as described earlier. The infected DRG neurons could be detected on day 7 after intrathecal delivery of LV-GFP or LV-shVILIP-1 to rats (Supplemental Fig. S5B). Using Western blot analysis, we found that knockdown of endogenous VILIP-1 by intrathecal delivery of LV-shVILIP-1 to rats also caused a marked reduction of P2X3 receptors in infected DRGs (74.6 ± 5.2% of naive, $P < .01$; 74.7 ± 3.0% of LV-GFP, $P < .01$, 1-way ANOVA, n = 4/group) (Fig. 6E). Moreover, using whole-cell patch clamp recording on IB4-positive DRG neurons, we found that knockdown of endogenous VILIP-1 dramatically reduced the α,β-meATP–evoked P2X3 currents (pA/pF) in contrast to naive or LV-GFP–infected rats (14.7 ± 1.7 LV-shVILIP-1 vs 26.2 ± 3.9 naive and 26.6 ± 3.2 LV-GFP, $P < .05$, 1-way ANOVA, n = 21/group) (Fig. 6F). Accordingly, α,β-meATP evoked fewer action potentials firing in LV-shVILIP-1–infected DRG neurons (Supplemental Table S5). Altogether, these data implied that knockdown of VILIP-1 functionally downregulated the P2X3 receptors in rat DRG neurons.

3.7. Pretreatment of LV-shVILIP-1 inhibits the development of bone cancer pain via functional downregulation of the P2X3 receptors and repression of the DRG neurons hyperexcitability in MRMT-1 rats

Given that knockdown of VILIP-1 functionally downregulates the P2X3 receptors and attenuates the DRG neuron excitability, we further investigated whether knockdown of VILIP-1 by pretreatment with LV-shVILIP-1 could preventively inhibit the development of bone cancer pain in MRMT-1 rats. Based on the aforementioned data that knockdown of VILIP-1 was achieved on day 7 after intrathecal delivery of LV-shVILIP-1 and that the cancer-induced pain behaviors appeared on approximately day 14 after tumor cell inoculation [46], we performed the knockdown of VILIP-1 pretreated by intrathecal delivery of LV-shVILIP-1 on day 7 and evaluated the pain behaviors on days 10, 14, 16, 18, and 20 after tumor cell inoculation. We observed that intrathecal delivery of LV-shVILIP-1 significantly inhibited the cancer-induced decreases in PWT (8.8 ± 1.8*g* LV-shVILIP-1/MRMT-1 vs 1.5 ± 0.2*g* MRMT-1 and 3.2 ± 0.6*g* LV-GFP/MRMT-1 at day 20, $P < .01$, 2-way ANOVA, n = 6–7/group) and PWL (15.4 ± 0.9 seconds LV-shVILIP-1/MRMT-1 vs 12.3 ± 1.3 seconds MRMT-1 and 11.0 ± 1.9 seconds LV-GFP/MRMT-1 at day 20, $P < .01$, 2-way ANOVA, n = 6/group) in MRMT-1 rats, indicating that preventive knockdown of VILIP-1 alleviated the cancer-induced mechanical allodynia and thermal hyperalgesia in MRMT-1 rats (Figs. 7A and 7B).

To further confirm whether the attenuated pain behaviors by pretreatment of LV-shVILIP-1 resulted from the functional downregulation of P2X3 receptors in DRG neurons, we examined the expression and function of P2X3 receptors as well as the DRG neurons excitability in those rats that had received the above-mentioned behavior tests. Indeed, Western blot analysis showed that intrathecal delivery of LV-shVILIP-1 inhibited both VILIP-1 (40.8 ± 8.0% of control, $P < .05$, unpaired *t* test, n = 3) and P2X3 receptors (38.1 ± 4.5% of control, $P < .01$, unpaired *t* test, n = 3) expression in MTMT-1 rat DRGs (Fig. 7C). Coincidently, using whole-cell patch clamp recording on IB4-positive DRG neurons, we found that the α,β-meATP–evoked P2X3 currents decreased significantly in MRMT-1 rats pretreated with LV-shVILIP-1 (21.6 ± 3.6 pA/pF, n = 15) compared with LV-GFP controls (37.1 ± 5.2 pA/pF, n = 21) ($P < .05$, unpaired *t* test; Fig. 7D). Moreover, we observed that the mean depolarization amplitude induced by α,β-meATP was significantly decreased in MRMT-1 rats pretreated with LV-shVILIP-1 (14.9 ± 1.3 mV, n = 19) compared with LV-GFP controls (19.5 ± 1.5 mV, n = 21) ($P < .05$, unpaired *t* test, Figs. 7E and 7F). As a result, intrathecal delivery of LV-shVILIP-1 greatly inhibited the α,β-meATP evoked action potentials firing in MRMT-1 rats (Fig. 7E). These results suggested that knockdown of VILIP-1 by pretreatment of LV-shVILIP-1 could preventively inhibit the development of bone cancer pain via functional downregulation of P2X3 receptors and repression of DRG neurons excitability in MRMT-1 rats.

3.8. Posttreatment of LV-shVILIP-1 alleviates the cancer-induced pain behaviors by functionally downregulating the P2X3 receptors in MRMT-1 rats

To further determine whether post-treatment with LV-shVILIP-1 could remedially alleviate the cancer-induced pain *behaviors* via

Fig. 5. Overexpression of visinin-like protein 1 (VILIP-1) elevates the expression and function of P2X3 receptors and enhances the neuronal excitability in rat dorsal root ganglion (DRG) neurons. (A–D) In cultured rat DRG neurons infected with lentivirus-VILIP-1-EGFP (LV-VILIP-1). (E–H) In dissociated DRGs from rats received intrathecal delivery of LV-VILIP-1 to infect DRG neurons. (A, B) Western blot of VILIP-1 overexpression. Note that overexpressed VILIP-1-EGFP (48 kDa) was detected using anti–green fluorescent protein (GFP) and glyceraldehyde 3-phosphate dehydrogenase (GAPDH) antibody (A) and anti-VILIP-1 antibody (B); expression of endogenous VILIP-1 (endo-VILIP-1, 22 kDa) was also detected using anti-VILIP-1 antibody (B, bottom band). (C) Immunostaining of P2X3 receptors in VILIP-1–overexpressed DRG neurons. Upper: GFP (green); lower: P2X3 receptors (red). Note that the immunofluorescence intensity of P2X3 receptors increased in LV-VILIP-1–infected cells (right bottom) compared with naive (left bottom) or LV-GFP (middle bottom) control, n = 4/group, scale bar = 7.5 μm. (D, E) Western blot of P2X3 receptor expression: in cultured DRG neurons (D); in dissociated DRGs (E). Upper: Representatives of Western blot bands; lower: analysis of the relative intensity of P2X3 receptors. Note that in both cultured DRG neurons and dissociated DRGs, P2X3 receptor expression increased dramatically in LV-VILIP-1–infected group, although endogenous VILIP-1 (endo-VILIP-1) was not significantly altered in all 3 groups: $^{**}P < .01$, compared with naive group; $^{\#}P < .05$, $^{\#\#}P < .01$ compared with the LV-GFP group, 1-way ANOVA, n = 4/group. (F) α,β-meATP–evoked fast-inactivating P2X3 currents in IB4(+) DRG neurons. Upper: Representatives of α,β-meATP– (20 μM for 3 seconds) evoked fast P2X3 currents. Lower: Summary of the current density (pA/pF). Note that overexpression of VILIP-1 significantly potentiated the α,β-meATP–evoked P2X3 currents, $^{**}P < .01$ compared with the naive group; $^{\#}P < .05$, compared with the LV-GFP group, 1-way ANOVA. (G, H) α,β-meATP–induced depolarization in IB4(+) DRG neurons. (G) Representatives of α,β-meATP–induced depolarization. Note that α,β-meATP evoked a greater depolarization and action potential firing in LV-VILIP-1–infected rats, indicating the enhancement of DRG neuron excitability in VILIP-1 overexpressed rats. (H) Summary of the mean depolarization amplitude. $^{**}p < .01$ compared with naive rats; $^{\#\#}P < .01$ compared with LV-GFP–infected rats, 1-way ANOVA. The numbers of recorded cells in each group are given in parentheses in each column of the panel.

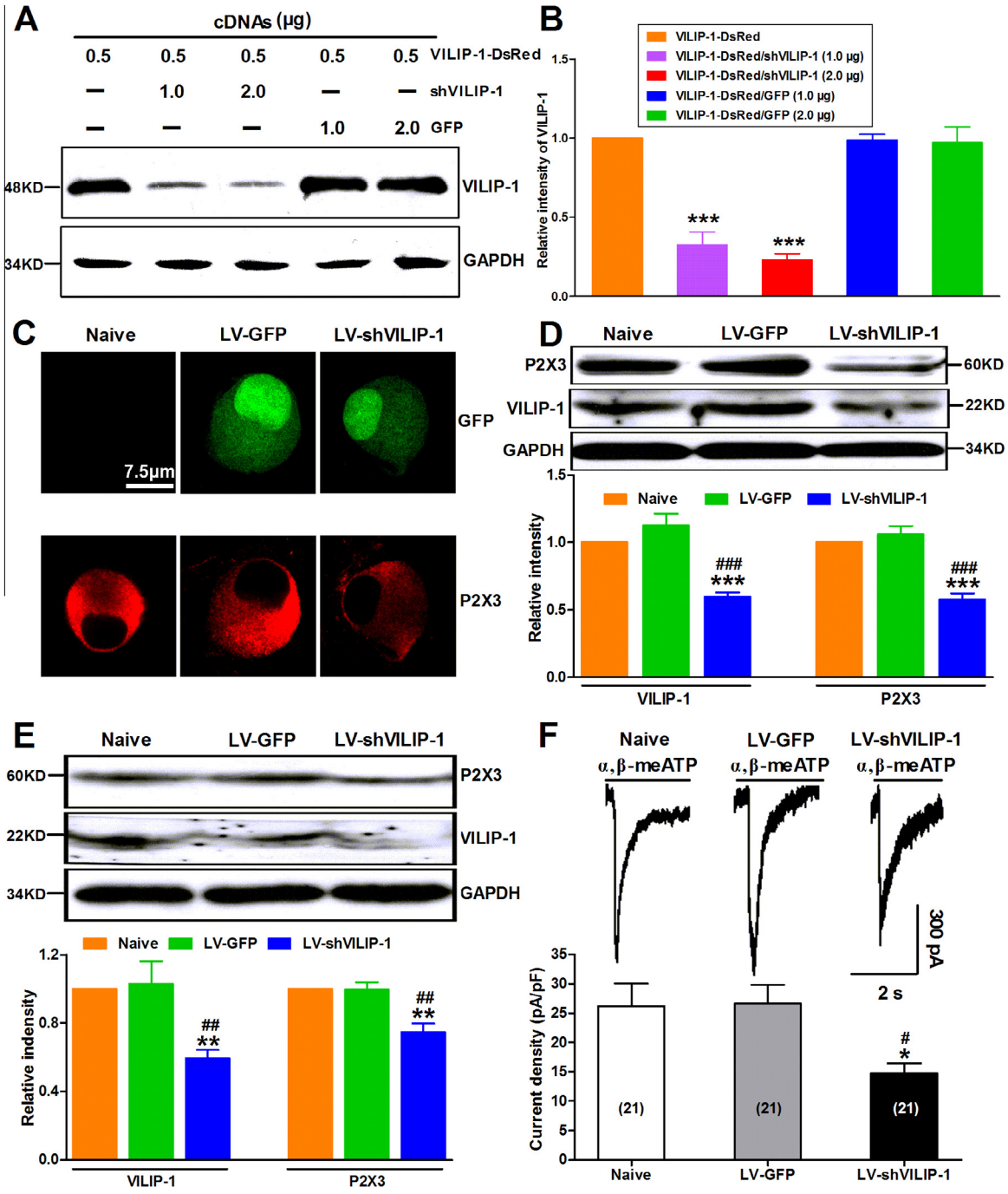

Fig. 6. Knockdown of visinin-like protein 1 (VILIP-1) reduces the expression and function of P2X3 receptors in rat dorsal root ganglion (DRG) neurons. (A, B) Assessment of VILIP-1 knockdown in HEK293 cells coexpressed VILIP-1-DsRed together with short hairpin VILIP-1 (shVILIP-1). (A) Representatives of Western blot bands on VILIP-1 expression. Glyceraldehyde 3-phosphate dehydrogenase (GAPDH) was used as internal control. The ratio of cotransfected plasmids was indicated in the panel. (B) Analysis of the relative intensity of VILIP-1. Note that the expression of VILIP-1 was markedly knocked down by transfection of shVILIP-1, $^{***}P < .001$, compared with green fluorescent protein (GFP) control, 1-way analysis of variance (ANOVA), n = 3. (C, D) Detection of P2X3 receptor expression in cultured rat DRG neurons infected with LV-shVILIP-1-GFP (LV-shVILIP-1). (E, F) Assessment of the expression and function of P2X3 receptors in dissociated DRGs from rats that received intrathecal delivery of LV-shVILIP-1 to infect DRG neurons. (C) Immunostaining of P2X3 receptors in cultured rat DRG neurons infected with LV-shVILIP-1 or LV-GFP. Upper: GFP (green); lower: P2X3 receptors (red). Note that the immunofluorescence intensity of P2X3 receptors decreased by knockdown of VILIP-1 in cells infected with LV-shVILIP-1 (right bottom) compared with naive (left bottom) or LV-GFP (middle bottom) control, n = 4/group, scale bar = 7.5 μm. (D, E) Western blot of P2X3 receptor expression: in cultured DRG neurons (D); in dissociated DRGs (E). Upper: representatives of Western blot bands, GAPDH was used as internal control; lower: analysis of the relative intensity of P2X3 receptors. Note that in both cultured DRG neurons and dissociated DRGs, the expression of P2X3 receptors decreased dramatically in association with a marked knockdown of VILIP-1 in the LV-shVILIP–1 infected group, $^{**}P < .01$, $^{***}P < .001$ compared with the naive group; $^{\#\#}P < .01$, $^{\#\#\#}P < .001$ compared with the LV-GFP group, 1-way ANOVA, n = 4/group. (F) α,β-meATP–evoked fast P2X3 currents in IB4(+) DRG neurons. Upper: representatives of α,β-meATP (20 μM for 3 seconds)-evoked fast P2X3 currents. Lower: summary of the current density (pA/pF). Note that knockdown of VILIP-1 by infecting LV-shVILIP-1 markedly suppressed the α,β-meATP–evoked currents, $^{*}P < .05$, compared with the naive group; $^{\#}P < .05$ compared with the LV-GFP group, 1-way ANOVA. The numbers of recorded cells in each group are given in parentheses in each column of the panel.

functional downregulation of the P2X3 receptors in MRMT-1 rats, we performed knockdown of VILIP-1 preventively by intrathecal delivery of LV-shVILIP-1 on day 11 and evaluated the pain behaviors on days 10, 14, 16, 18, and 20 after tumor cell inoculation. We inferred that obvious knockdown of VILIP-1 appeared on approximately day 18 after tumor cell inoculation when

apparent pain behaviors had already occurred because knockdown of VILIP-1 was achieved on day 7 after intrathecal delivery of LV-shVILIP-1 and the cancer-induced pain behaviors appeared on day 14 after tumor cell inoculation [46]. As expected, post-treatment with LV-shVILIP-1 significantly inhibited the cancer-induced decrease in PWT (6.7 ± 1.1 g LV-shVILIP-1/MRMT-1 vs 1.5 ± 0.2 g MRMT-1 and 2.3 ± 0.6 g LV-GFP/MRMT-1 at day 20, $P < .01$, 2-way ANOVA, n = 6–9/group) (Fig. 8A), and to some extent, also temporarily inhibited the cancer-induced decrease in PWL (14.4 ± 2.0 seconds LV-shVILIP-1/MRMT-1 vs 11.3 ± 1.3 seconds MRMT-1 and 9.1 ± 0.6 seconds LV-GFP/MRMT-1 at day 16, $P < .01$, 2-way ANOVA, n = 5–9/group) (Fig. 8B), indicating that preventive knockdown of VILIP-1 could remedially alleviate the cancer-induced mechanical allodynia in MRMT-1 rats.

Finally, the expression and function of P2X3 receptors in those rats that underwent the above-mentioned behavior test were further studied. Similarly, we found that post-treatment of LV-shVILIP-1 inhibited both VILIP-1 (50.2 ± 1.8% of control, $P < .01$,

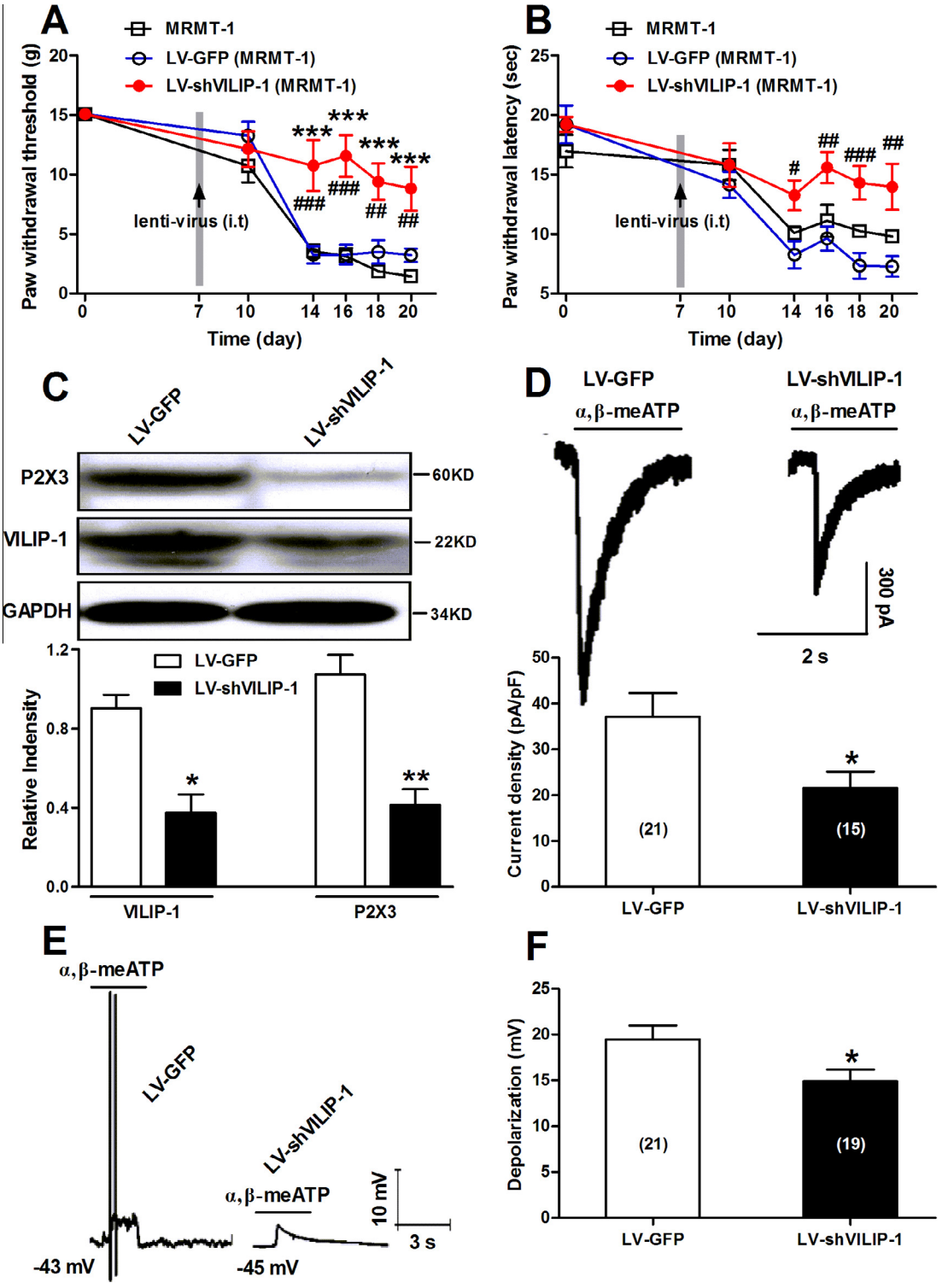

unpaired *t* test, n = 3) and P2X3 receptors (60.8 ± 2.3% of control, $P < .01$, unpaired *t* test, n = 3) expression in MTMT-1 rat DRGs (Fig. 8C). Additionally, using whole-cell patch clamp recording on IB4-positive DRG neurons, we also found that the α,β-meATP–evoked P2X3 currents decreased significantly in MRMT-1 rats post-treated with LV-shVILIP-1 (20.0 ± 3.1 pA/pF, n = 22) as compared with LV-GFP controls (34.8 ± 5.2 pA/pF, n = 22) ($P < 0.05$, unpaired *t* test, Fig. 8D). These results indicated that knockdown of VILIP-1 by post-treatment of LV-shVILIP-1 could remedially alleviate cancer-induced pain behaviors by functional downregulation of P2X3 receptors in MRMT-1 rats.

4. Discussion

In this study, we disclosed a novel molecular mechanism underlying the functional upregulation of P2X3 receptors in cancer rat DRG neurons, which is associated with the neuronal hyperexcitability and the cancer-induced bone pain: VILIP-1, one of the neuronal calcium sensor proteins that was first detected in DRG neurons in our study, interacted with P2X3 receptor C-terminus and enhanced the expression and function of the receptor, which in turn caused the hyperexcitation of DRG neurons that is proposed to underlie the pathogenesis of cancer-induced bone pain. Overexpression of VILIP-1 increased the expression and function of P2X3 receptors and enhanced the excitability of DRG neurons; whereas knockdown of VILIP-1 attenuated the cancer-induced pain behaviors via functional downregulation of P2X3 receptors and repression of DRG neuron hyperexcitability in cancer rats. Thus, functional upregulation of P2X3 receptors by VILIP-1 in DRG neurons contributes to the cancer-induced bone pain in rats.

4.1. Functional upregulation of P2X3 receptors in DRG neurons contributes to the development of bone cancer pain in MRMT-1 rats

Here we provide evidence that the expression of P2X3 receptors significantly increased in MRMT-1 rat DRGs. We detected a marked increase both in total and membrane P2X3 receptor expression in cancer rat DRGs, consistent with previous findings that increased expression of P2X3 receptors was seen in various models of chronic pain [31,40,41]. In support of the role of P2X3 receptors in nociception and persistent pain [4,19,38–40], we observed that the increased P2X3 receptors appeared from days 14 to 28 after tumor cell inoculation, which temporally correlates with the occurrence of cancer-induced pain behaviors [46].

In line with the increase in P2X3 receptor expression in cancer rat DRGs, we found a marked increase in the current density of agonist (α,β-meATP)-evoked fast-inactivating P2X3 currents in MRMT-1 rat DRG neurons. Possible mechanisms for the potentiation of fast-inactivating P2X3 currents include an increase of single-channel conductance, an enhancement of open probability, an augmentation of the affinity to agonist, and/or an increase in functional P2X3 receptor expression [42]. Although single P2X3 receptor channel properties in cancer rat DRG neurons have not been studied, an increase in the opening probability of P2X3 receptor channels was probably not possible because the kinetic properties of P2X3 currents remained unchanged in bone cancer rats. Moreover, an augmentation of the affinity to agonist could also be excluded because the half maximal effective concentration for activation of P2X3 receptors by α,β-meATP was not significantly altered in MRMT-1 rat DRG neurons. Thus, the increased expression of P2X3 receptors would be the determining factor for the potentiation of fast-inactivating P2X3 currents in bone cancer rats [40,41]. The enhanced P2X3 currents gave rise to a greater depolarization in MRMT-1 rat DRG neurons; among them, ~50% of the depolarization was great enough to evoke action potentials, implying that the potentiation of fast-inactivating P2X3 currents likely mediated the hyperexcitability of cancer rat DRG neurons that may underlie the pathogenesis of cancer-induced bone pain. Based on our behavioral findings and those of the previous study by Kaan et al. [21], who reported that blockade of P2X3 and P2X2/3 receptors on both the peripheral and central terminals of nociceptors contributes to analgesic efficacy in a rat model of bone cancer pain, we propose that functional upregulation of P2X3 receptors mediates the hyperexcitability of DRG neurons, which in turn contributes to the development of cancer-induced bone pain in MRMT-1 rats [40,46].

4.2. Regulation of P2X3 receptors by VILIP-1: implications and mechanisms

Considerable evidence has accumulated that VILIP-1, a member of the family of neuronal calcium sensor proteins, mainly expressed in the brain as reported previously [25], may function as a general regulator of ligand-gated ion channels that affects the surface expression and function of the receptors [3,8]. In this study, we demonstrated for the first time to our knowledge that VILIP-1 was universally expressed, in terms of both protein and mRNA levels, in naive rat DRG neurons. Upregulation of VILIP-1 expression was further confirmed in bone cancer rats, and, most interestingly, the increased expression of VILIP-1 was found to temporally accompany with the elevation of P2X3 receptors in the time line following tumor cells inoculation. These data strongly suggest that increased VILIP-1 may act as a regulator of P2X3 receptors, causing a functional upregulation of the receptors under cancer condition [8,40]. Indeed, we identified the interaction between VILIP-1 and the P2X3 receptor C-terminus, in both HEK293 cells and rat DRG neurons. In addition, we further demonstrated that the NT1–22 aa domain containing *N*-myristoyl glycine2 in VILIP-1 is required

Fig. 7. Pre-treatment of lentivirus short hairpin visinin-like protein 1 (LV-shVILIP-1) inhibits the cancer-induced pain behaviors, reduces the expression and function of P2X3 receptors, and represses dorsal root ganglion (DRG) neuron excitability in MRMT-1 rats. (A, B) Effects of intrathecal (i.t.) delivery of LV-shVILIP-1 on mechanical allodynia (A) and thermal hyperalgesia (B) in MTMT-1 rats. LV-shVILIP-1 or LV-green fluorescent protein (GFP) was intrathecally administered to MRMT-1 rats on day 7 after tumor cell inoculation (ie, before the appearance of cancer-induced pain behaviors [arrow]). Note that i.t. delivery of LV-shVILIP-1 significantly inhibited the cancer-induced decreases in mechanical allodynia (as measured by paw withdrawal threshold) and thermal hyperalgesia (as measured by paw withdrawal latency) in MRMT-1 rats, indicating that knockdown of VILIP-1 effectively inhibited the cancer-induced pain behaviors in MRMT-1 rats. $^{***}P < .001$ compared with MRMT-1 group; $^{\#}P < .05$, $^{\#\#}P < .01$, $^{\#\#\#}P < .001$ compared with LV-GFP group, 2-way analysis of variance (ANOVA), n = 6–9/group. (C) Effects of intrathecal delivery of LV-shVILIP-1 on expression of VILIP-1 and P2X3 receptors in MTMT-1 rat DRGs. Upper: representatives of Western blot bands, glyceraldehyde 3-phosphate dehydrogenase (GAPDH) was used as internal control; lower: analysis of the relative intensity of VILIP-1 and P2X3 receptors. Note that i.t. delivery of LV-shVILIP-1 inhibited both VILIP-1 and P2X3 receptor expression in MTMT-1 rat DRGs. $^{*}P < .05$, $^{**}P < .01$ compared with LV-GFP groups, unpaired *t* test, n = 3. (D) Effects of i.t. delivery of LV-shVILIP-1 on α,β-meATP–evoked P2X3 currents in IB4(+) DRG neurons in MRMT-1 rats. Upper: representatives of α,β-meATP– (20 μM for 3 seconds) evoked fast P2X3 currents. Lower: summary of the current density (pA/pF). Note that knockdown of VILIP-1 via i.t. delivery of LV-shVILIP-1 markedly reduced the α,β-meATP–evoked P2X3 currents, $^{*}P < .05$ compared with the LV-GFP group, unpaired *t* test. (E, F) α,β-meATP–induced depolarization in IB4(+) DRG neurons in MRMT-1 rats. (E) Representatives of α,β-meATP–induced depolarization. Note that α,β-meATP evoked less depolarization that insufficiently elicits action potential firing in LV-shVILIP-1 rats, indicating that knockdown of VILIP-1 dramatically repressed the DRG neuron excitability in bone cancer rats. (F) Summary of the mean depolarization amplitude. $^{*}P < .05$ compared with the LV-GFP group, unpaired *t* test. The numbers of recorded cells in each group are given in parentheses in each column of the panel.

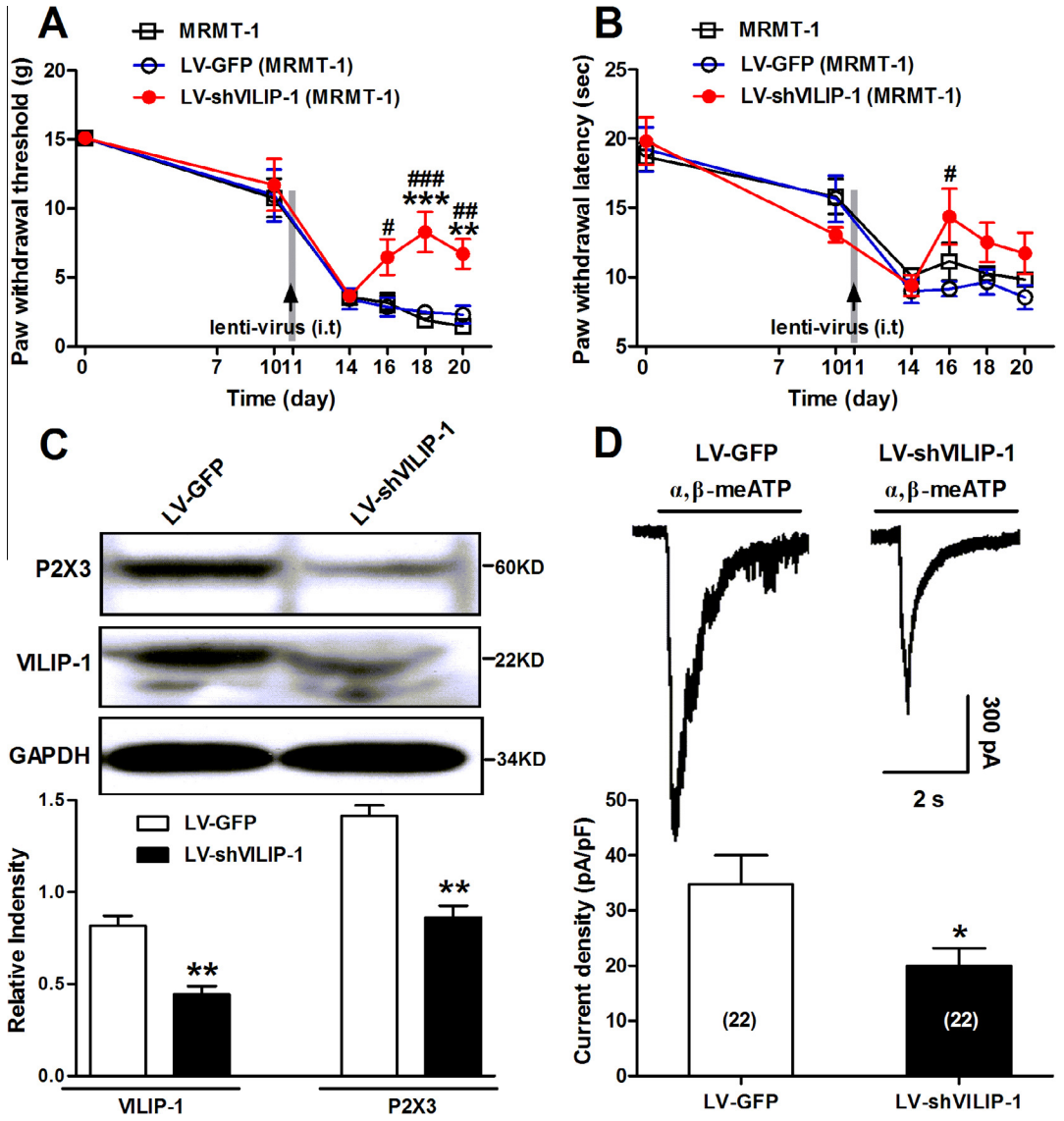

Fig. 8. Post-treatment of lentivirus short hairpin visinin-like protein 1 (LV-shVILIP-1) alleviates the cancer-induced pain behaviors and reduces the expression and function of P2X3 receptors in MRMT-1 rats. (A, B) Effects of post-treated LV-shVILIP-1 on mechanical allodynia (A) and thermal hyperalgesia (B) in MTMT-1 rats. LV-shVILIP-1 or LV-green fluorescent protein (GFP) was intrathecally) administered to MRMT-1 rats on day 11 after tumor cell inoculation (ie, after the occurrence of cancer-induced pain behaviors [arrow]). Note that intrathecal (i.t.) delivery of LV-shVILIP-1 significantly inhibited the cancer-induced decrease in paw withdrawal threshold to von Frey filaments rather than paw withdrawal latency to radiant heat, indicating that knockdown of VILIP-1 by post-treatment of LV-shVILIP-1 dramatically alleviated the cancer-induced mechanical allodynia in MRMT-1 rats. $^{**}P < .01$, $^{***}P < .001$ compared with MRMT-1 group; $^{\#}P < .05$, $^{\#\#}P < .01$, $^{\#\#\#}P < .001$ compared with LV-GFP group, 2-way analysis of variance, n = 6–9/group. (C) Effects of i.t. delivery of LV-shVILIP-1 on expressions of VILIP-1 and P2X3 receptors in MTMT-1 rat DRGs. Upper: representative of Western blot bands, glyceraldehyde 3-phosphate dehydrogenase (GADPH) was used as internal control; lower: analysis of the relative intensity of VILIP-1 and P2X3 receptors. Note that i.t. delivery of LV-shVILIP-1 inhibited both VILIP-1 and P2X3 receptor expression in MTMT-1 rat DRGs. $^{**}P < .01$ compared with i.t. LV-GFP groups, unpaired *t* test, n = 3. (D) Effects of i.t. delivery of LV-shVILIP-1 on α,β-meATP–evoked P2X3 currents in IB4(+) DRG neurons in MTMT-1 rats. Upper: representatives of α,β-meATP– (20 μM for 3 seconds) evoked fast P2X3 currents. Lower: summary of the current density (pA/pF). Note that knockdown of VILIP-1 by post-treatment of LV-shVILIP-1 suppressed the α,β-meATP–evoked currents, $^{*}P < .05$ compared with the LV-GFP group, unpaired *t* test. The numbers of recorded cells in each group are given in parentheses in each column of the panel.

for their interaction, supporting the notion that VILIP-1 may form a signaling complex with its binding receptors [8,12,27,44].

Interaction of VILIP-1 with α4β2 nAChRs or P2X2 receptors enhances the surface expression and function of the receptors [8,27,44]. Here we present in vitro and in vivo evidence that similar effects can be observed due to interactions between VILIP-1 and P2X3 receptors. In HEK293 cells, VILIP-1 enhances the expression of P2X3 receptors and potentiates the α,β-meATP–evoked P2X3 currents, whereas a mutant, mVILIP-1-myr, has no such effect. In rat DRG neurons, overexpression of VILIP-1 increases the expression and function of P2X3 receptors and therefore enhances the neuronal excitability; in contrast, knockdown of VILIP-1 produces the opposite effects. Our data uncover a potential molecular mechanism underlying the functional upregulation of P2X3 receptors in bone cancer rats.

4.3. Upregulation of P2X3 receptors by VILIP-1 contributes to the development of bone cancer pain

Given that functional upregulation of P2X3 receptors mediates the hyperexcitability of cancer rat DRG neurons that is suggested to underlie the pathogenesis of cancer-induced bone pain [46],

we hypothesized that the regulation of P2X3 receptors by VILIP-1, which is proposed to affect the expression and function of the receptors as well as the DRG neurons excitability, might play a crucial role in the development of bone cancer pain. In this study, we provide direct evidence that knockdown of VILIP-1 by intrathecal delivery of LV-shVILIP-1 inhibits the development of bone cancer pain in MRMT-1 rats via functional downregulation of P2X3 receptors and repression of DRG neuron excitability. Thus, functional upregulation of P2X3 receptors by VILIP-1 in DRG neurons is likely involved in the pathogenesis of bone cancer pain in rats. Certainly, the role of other channels or receptors in a model of bone cancer pain, which might also be regulated by VILIP-1 in DRG neurons [15,27,29], remains to be further studied. In the case that the enhancement of other channels regulated by VILIP-1 could be identified in cancer rat DRG neurons, knockdown of VILIP-1 in DRGs would be well qualified as a potential target for the treatment of bone cancer pain. Here, we propose that functional upregulation of P2X3 receptors by VILIP-1 in DRG neurons makes a significant contribution to cancer-induced bone pain in a rat model. However, we are unable so far to exclude the contribution of such regulation in the spinal cord dorsal horn. We observed that in the dorsal horn of the spinal cord, the expression of P2X3 receptors was up-regulated, whereas no alteration was observed on VILIP-1 expression (data not shown) in bone cancer rats. Although our data demonstrate that intrathecal delivery of LV-VILIP-1 or LV-shVILIP-1 could respectively achieve overexpression or knockdown of VILIP-1 in DRG neurons, which in turn causing functional upregulation or downregulation of the P2X3 receptors in DRG neurons, overexpression or knockdown of VILIP-1 in the dorsal horn neurons would not be excluded in our experiments. Hence, in the spinal cord dorsal horn, the contribution of VILIP-1–mediated modulation of P2X3 receptors to the cancer pain needs to be further studied.

4.4. Conclusions

Our data provide a novel molecular mechanism underlying the functional upregulation of P2X3 receptors in bone cancer rats: VILIP-1, a member of the family of neuronal calcium sensor proteins, interacts with the C-terminal tail of the P2X3 receptor and enhances the expression and function of the receptor, which in turn causes the hyperexcitation of DRG neurons, which is proposed to underlie the pathogenesis of cancer-induced bone pain. These results suggest that functional upregulation of P2X3 receptors by VILIP-1 in DRG neurons contributes to the development of bone cancer pain in MRMT-1 rats. Hence, P2X3 receptors and VILIP-1 may serve as promising targets for therapeutic interventions in cancer patients for pain management. Pharmacological blockade of P2X3 receptors or knockdown of VILIP-1 in DRG neurons could be used as innovative strategies for the treatment of bone cancer pain.

Conflict of interest statement

The authors have no conflicts of interest to report.

Acknowledgments

This work was supported by grants from the National Natural Science Foundation of China (31171063, 81072951, and 61027001), the Beijing Natural Science Foundation (7112079), the special foundation for public welfare profession scientific research program from Ministry of Health of the Peoples Republic of China (201302013-01), and the 973 Program of the Ministry of Science and Technology of China (2013CB531905). We thank Dr. Alan North (Manchester University, Manchester, England) for providing the wtP2X3 receptor plasmid; Dr. F. Coussen (Institute for Interdisciplinary Neuroscience, Bordeaux, France) and Dr. Karl-Heinz Braunewell (Southern Research Institute, Birmingham, Alabama) for providing wtVILIP-1 plasmids; Dr. Li Liu (Sichuan Agricultural University, Sichuan, China) for providing all types of empty vectors in molecular biology; Dr. Albert Cheung Hoi Yu (Neuroscience Research Institute of Peking University, Beijing, China) for providing the ABI7500 real-time PCR equipment. We thank Dr. Xiaodong Liu in Department of Biomedical Engineering, School of Medicine, Tsinghua University, Beijing, China, and Angela A. Song, Columbia University, New York, New York, for their kind help in the preparation of this manuscript.

Appendix A. Supplementary data

Supplementary data associated with this article can be found, in the online version, at http://dx.doi.org/10.1016/j.pain.2013.04.022.

References

[1] Bao L, Jin SX, Zhang C, Wang LH, Xu ZZ, Zhang FX, Wang LC, Ning FS, Cai HJ, Guan JS, Xiao HS, Xu ZQ, He C, Hokfelt T, Zhou Z, Zhang X. Activation of delta opioid receptors induces receptor insertion and neuropeptide secretion. Neuron 2003;37:121–33.
[2] Bland-Ward PA, Humphrey PP. P2X receptors mediate ATP-induced primary nociceptive neurone activation. J Auton Nerv Syst 2000;81:146–51.
[3] Braunewell KH, Klein-Szanto AJ. Visinin-like proteins (VSNLs): interaction partners and emerging functions in signal transduction of a subfamily of neuronal Ca2+-sensor proteins. Cell Tissue Res 2009;335:301–16.
[4] Brederson JD, Jarvis MF. Homomeric and heteromeric P2X3 receptors in peripheral sensory neurons. Curr Opin Investig Drugs 2008;9:716–25.
[5] Burgard EC, Niforatos W, Van BT, Lynch KJ, Touma E, Metzger RE, Kowaluk EA, Jarvis MF. P2X receptor-mediated ionic currents in dorsal root ganglion neurons. J Neurophysiol 1999;82:1590–8.
[6] Burnstock G. Purinergic P2 receptors as targets for novel analgesics. Pharmacol Ther 2006;110:433–54.
[7] Chaplan SR, Bach FW, Pogrel JW, Chung JM, Yaksh TL. Quantitative assessment of tactile allodynia in the rat paw. J Neurosci Methods 1994;53:55–63.
[8] Chaumont S, Compan V, Toulme E, Richler E, Housley GD, Rassendren F, Khakh BS. Regulation of P2X2 receptors by the neuronal calcium sensor VILIP1. Sci Signal 2008;1:ra8.
[9] Chen Y, Li GW, Wang C, Gu Y, Huang LY. Mechanisms underlying enhanced P2X receptor-mediated responses in the neuropathic pain state. PAIN® 2005;119:38–48.
[10] Chizh BA, Illes P. P2X receptors and nociception. Pharmacol Rev 2001;53:553–68.
[11] Coddou C, Yan Z, Obsil T, Huidobro-Toro JP, Stojilkovic SS. Activation and regulation of purinergic P2X receptor channels. Pharmacol Rev 2011;63:641–83.
[12] Coussen F, Perrais D, Jaskolski F, Sachidhanandam S, Normand E, Bockaert J, Marin P, Mulle C. Co-assembly of two GluR6 kainate receptor splice variants within a functional protein complex. Neuron 2005;47:555–66.
[13] Dixon WJ. Efficient analysis of experimental observations. Annu Rev Pharmacol Toxicol 1980;20:441–62.
[14] Dowd E, McQueen DS, Chessell IP, Humphrey PP. P2X receptor-mediated excitation of nociceptive afferents in the normal and arthritic rat knee joint. Br J Pharmacol 1998;125:341–6.
[15] Few AP, Lautermilch NJ, Westenbroek RE, Scheuer T, Catterall WA. Differential regulation of CaV2.1 channels by calcium-binding protein 1 and visinin-like protein-2 requires N-terminal myristoylation. J Neurosci 2005;25:7071–80.
[16] Geng SJ, Liao FF, Dang WH, Ding X, Liu XD, Cai J, Han JS, Wan Y, Xing GG. Contribution of the spinal cord BDNF to the development of neuropathic pain by activation of the NR2B-containing NMDA receptors in rats with spinal nerve ligation. Exp Neurol 2010;222:256–66.
[17] Huang ZJ, Song XJ. Differing alterations of sodium currents in small dorsal root ganglion neurons after ganglion compression and peripheral nerve injury. Mol Pain 2008;4:20.
[18] Ihara M, Yamasaki N, Hagiwara A, Tanigaki A, Kitano A, Hikawa R, Tomimoto H, Noda M, Takanashi M, Mori H, Hattori N, Miyakawa T, Kinoshita M. Sept4, a component of presynaptic scaffold and Lewy bodies, is required for the suppression of alpha-synuclein neurotoxicity. Neuron 2007;53:519–33.
[19] Jarvis MF. Contributions of P2X3 homomeric and heteromeric channels to acute and chronic pain. Expert Opin Ther Targets 2003;7:513–22.
[20] Jimenez-Andrade JM, Mantyh WG, Bloom AP, Ferng AS, Geffre CP, Mantyh PW. Bone cancer pain. Ann N Y Acad Sci 2010;1198:173–81.
[21] Kaan TK, Yip PK, Patel S, Davies M, Marchand F, Cockayne DA, Nunn PA, Dickenson AH, Ford AP, Zhong Y, Malcangio M, McMahon SB. Systemic blockade of P2X3 and P2X2/3 receptors attenuates bone cancer pain behaviour in rats. Brain 2010;133:2549–64.

[22] Kaczmarek-Hajek K, Lorinczi E, Hausmann R, Nicke A. Molecular and functional properties of P2X receptors – recent progress and persisting challenges. Purinergic Signal 2012;8:375–417.
[23] Kage K, Niforatos W, Zhu CZ, Lynch KJ, Honore P, Jarvis MF. Alteration of dorsal root ganglion P2X3 receptor expression and function following spinal nerve ligation in the rat. Exp Brain Res 2002;147:511–9.
[24] Kim C, Chung JM, Chung K. Changes in the gene expression of six subtypes of P2X receptors in rat dorsal root ganglion after spinal nerve ligation. Neurosci Lett 2003;337:81–4.
[25] Kuno T, Kajimoto Y, Hashimoto T, Mukai H, Shirai Y, Saheki S, Tanaka C. CDNA cloning of a neural visinin-like Ca(2+)-binding protein. Biochem Biophys Res Commun 1992;184:1219–25.
[26] Lampert A, Dib-Hajj SD, Tyrrell L, Waxman SG. Size matters: Erythromelalgia mutation S241T in Nav1.7 alters channel gating. J Biol Chem 2006;281: 36029–35.
[27] Lin L, Jeanclos EM, Treuil M, Braunewell KH, Gundelfinger ED, Anand R. The calcium sensor protein visinin-like protein-1 modulates the surface expression and agonist sensitivity of the alpha 4beta 2 nicotinic acetylcholine receptor. J Biol Chem 2002;277:41872–8.
[28] Medhurst SJ, Walker K, Bowes M, Kidd BL, Glatt M, Muller M, Hattenberger M, Vaxelaire J, O'Reilly T, Wotherspoon G, Winter J, Green J, Urban L. A rat model of bone cancer pain. PAIN® 2002;96:129–40.
[29] Nakamura TY, Pountney DJ, Ozaita A, Nandi S, Ueda S, Rudy B, Coetzee WA. A role for frequenin, a Ca2+-binding protein, as a regulator of Kv4 K+-currents. Proc Natl Acad Sci U S A 2001;98:12808–13.
[30] Natura G, von Banchet GS, Schaible HG. Calcitonin gene-related peptide enhances TTX-resistant sodium currents in cultured dorsal root ganglion neurons from adult rats. PAIN® 2005;116:194–204.
[31] Novakovic SD, Kassotakis LC, Oglesby IB, Smith JA, Eglen RM, Ford AP, Hunter JC. Immunocytochemical localization of P2X3 purinoceptors in sensory neurons in naive rats and following neuropathic injury. PAIN® 1999;80: 273–82.
[32] Petruska JC, Cooper BY, Johnson RD, Gu JG. Distribution patterns of different P2x receptor phenotypes in acutely dissociated dorsal root ganglion neurons of adult rats. Exp Brain Res 2000;134:126–32.
[33] Qu XX, Cai J, Li MJ, Chi YN, Liao FF, Liu FY, Wan Y, Han JS, Xing GG. Role of the spinal cord NR2B-containing NMDA receptors in the development of neuropathic pain. Exp Neurol 2009;215:298–307.
[34] Ren Y, Zou X, Fang L, Lin Q. Involvement of peripheral purinoceptors in sympathetic modulation of capsaicin-induced sensitization of primary afferent fibers. J Neurophysiol 2006;96:2207–16.
[35] Surprenant A, North RA. Signaling at purinergic P2X receptors. Annu Rev Physiol 2009;71:333–59.
[36] Towne C, Pertin M, Beggah AT, Aebischer P, Decosterd I. Recombinant adeno-associated virus serotype 6 (rAAV2/6)-mediated gene transfer to nociceptive neurons through different routes of delivery. Mol Pain 2009;5:52.
[37] Tsuzuki K, Kondo E, Fukuoka T, Yi D, Tsujino H, Sakagami M, Noguchi K. Differential regulation of P2X(3) mRNA expression by peripheral nerve injury in intact and injured neurons in the rat sensory ganglia. PAIN® 2001;91: 351–60.
[38] Wirkner K, Sperlagh B, Illes P. P2X3 receptor involvement in pain states. Mol Neurobiol 2007;36:165–83.
[39] Wu G, Whiteside GT, Lee G, Nolan S, Niosi M, Pearson MS, Ilyin VI. A-317491, a selective P2X3/P2X2/3 receptor antagonist, reverses inflammatory mechanical hyperalgesia through action at peripheral receptors in rats. Eur J Pharmacol 2004;504:45–53.
[40] Wu JX, Xu MY, Miao XR, Lu ZJ, Yuan XM, Li XQ, Yu WF. Functional up-regulation of P2X3 receptors in dorsal root ganglion in a rat model of bone cancer pain. Eur J Pain 2012;16:1378–88.
[41] Xiang Z, Xiong Y, Yan N, Li X, Mao Y, Ni X, He C, LaMotte RH, Burnstock G, Sun J. Functional up-regulation of P2X 3 receptors in the chronically compressed dorsal root ganglion. PAIN® 2008;140:23–34.
[42] Xu GY, Huang LY. Peripheral inflammation sensitizes P2X receptor-mediated responses in rat dorsal root ganglion neurons. J Neurosci 2002; 22:93–102.
[43] Zhao C, Anand R, Braunewell KH. Nicotine-induced Ca2+-myristoyl switch of neuronal Ca2+ sensor VILIP-1 in hippocampal neurons: a possible crosstalk mechanism for nicotinic receptors. Cell Mol Neurobiol 2009;29: 273–86.
[44] Zhao CJ, Noack C, Brackmann M, Gloveli T, Maelicke A, Heinemann U, Anand R, Braunewell KH. Neuronal Ca2+ sensor VILIP-1 leads to the upregulation of functional alpha4beta2 nicotinic acetylcholine receptors in hippocampal neurons. Mol Cell Neurosci 2009;40:280–92.
[45] Zhao J, Pan HL, Li TT, Zhang YQ, Wei JY, Zhao ZQ. The sensitization of peripheral C-fibers to lysophosphatidic acid in bone cancer pain. Life Sci 2010;87:120–5.
[46] Zheng Q, Fang D, Cai J, Wan Y, Han JS, Xing GG. Enhanced excitability of small dorsal root ganglion neurons in rats with bone cancer pain. Mol Pain 2012;8:24–41.
[47] Zimmermann M. Pathobiology of neuropathic pain. Eur J Pharmacol 2001; 429:23–37.
[48] Zimmermann M. Ethical guidelines for investigations of experimental pain in conscious animals. PAIN® 1983;16:109–10.